

MPD NICA

Technical Design Report

of the

Time of Flight System (TOF)

TOF Group of the MPD Collaboration

Laboratory of High Energy Physics, JINR, Dubna:

V.A. Babkin, S.N. Bazylev, A.S. Burdyko, M.G. Buryakov, S.G. Buzin, P.V. Chumakov, V.M. Golovatyuk, A.V. Dmitriev, P.O. Dulov, D.S. Egorov, Yu.I. Fedotov, S.I. Kakurin, V.I. Kolesnikov, S.P. Lobastov, V.A. Petrov, I.A. Philippov, M. Piatek, M.M. Rummyantsev, V.M. Slepnev, I.V. Slepnev, D.V. Shchegolev, A.V. Shutov, V.B. Shutov, A.V. Shipunov, S.I. Sukhovarov, A.V. Terletskiy, S.V. Volgin, N.M. Vladimirova.

Warsaw University of Technology, Warsaw, Poland:

M. Czarnynoga, D. Dąbrowski, M. Kutyla, M.J. Peryt, K. Roslon.

B. I. Stepanov Institute of Physics, NASB, Minsk, Belarus:

A.V. Litomin.

Department of Engineering Physics, Tsinghua University, Beijing, China:

Yi Wang, Zhu Weiping, Yuanjing Li, Yinong Liu, Zhi Deng, Guanghua Gong, Xianglei Zhu, Weicheng Ding.

Center of Particle Physics and Technology (CPPT) of the University of Science and Technology of China (USTC) Hefei, China:

Cheng Li, Hongfang Chen, Ming Shao, Xiaoliang Wang, Yongjie Sun, Zebo Tang.

Laboratory of Radiation Research, Belgorod National Research University, Belgorod:

V.I. Dronik, A.S. Klyuev, A.S. Kubankin, A.D. Pyatigor, K.A. Vokhmyanina.

Contents

1	Introduction	4
1.1	The MPD experiment	4
1.2	Particles identification in the MPD	6
1.3	Requirements for the TOF system	6
1.3.1	<i>The basic requirements</i>	6
1.3.2	<i>The particles separation performance of the TOF</i>	7
1.3.3	<i>Occupancy and counting rate estimation</i>	9
2	Development of the MRPC for the TOF	11
2.1	Motivation of choosing the MRPC for the TOF system	11
2.2	Designs of the MRPC prototypes	11
2.3	Beam setup and cosmic stand for testing detectors	13
2.4	Test results	15
2.5	Study of rate capabilities of a MRPC	16
3	The MPD TOF system design	18
3.1	Detail layout of the MRPC for the MPD time-of-flight system.	18
3.2	Mechanical design of the TOF barrel	21
3.3	The occupancy and geometric efficiency of the TOF system.	24
3.4	Acceptance estimation and track matching	26
3.5	Time-of-Flight particles identification performance	29
3.6	Front-end electronics and data acquisition system	30
3.6.1	<i>Preamplifiers for the TOF MRPC</i>	30
3.6.2	<i>Preamplifier's voltage supply</i>	35
3.6.3	<i>Preamplifier's control</i>	35
3.6.4	<i>Time-Over-Threshold method</i>	37
3.6.5	<i>Time-to-digital converter TDC72VHL</i>	38
3.7	Weight and material budget of the TOF system	39
3.8	Area for mass-production of the TOF MRPC	40
3.9	Step-by-step MRPC assembling procedure	42
3.10	TOF modules installation	46
4	Service	49
4.1	Gas system	49
4.1.1	<i>Simple gas system for testing elements of the TOF</i>	49
4.1.2	<i>Proposed closed loop circulation gas system</i>	50
4.2	High Voltage supplies	54
4.3	Low Voltage power distribution	55
4.4	Slow control for the TOF system	56
4.5	Power consumption and cooling	58
5	Organization and cost estimation	59
5.1	Organization	59
5.2	Cost and resources	59
5.3	The time schedule	60
	References	61

1 Introduction

1.1 The MPD experiment

The MPD is designed as a 4π -spectrometer capable of detecting charged hadrons, electrons and photons in heavy-ion collisions in the energy range of the NICA collider [1, 2]. To reach this goal, the detector will include a precise 3D tracking system and a high-performance particle identification system based on time-of-flight measurements and calorimetry. At the design luminosity, the event rate in the MPD interaction region is about 6 kHz; the total charged particle multiplicity exceeds 1000 in the most central Au+Au collisions at $\sqrt{s_{NN}} = 11$ GeV. As the average transverse momentum of the particles produced in a collision at the NICA energies is below 500 MeV/c, the detector design requires a very low material budget. The general layout of the MPD apparatus is shown in Fig. 1.1.

The Multi-Purpose Detector consists of a barrel part and two endcaps located inside the magnetic field. The barrel part is a shell-like set of various detector systems surrounding the interaction point and aimed at reconstructions and identifying both charged and neutral particles in the pseudorapidity region of $|\eta| \leq 1.3$. The endcaps are aimed at the precise tracking over pseudo-rapidity range ($1.3 < |\eta| < 2$). The ion beams interact inside the beam pipe located along the z axis with the central interaction point at $z = 0$ in the center of the detector. The interaction region covers an interval of $|z| \leq 25$ cm.

The barrel part shown in Fig. 1.1 consists of a tracker and particle identification system. The principal tracker is the time projection chamber (TPC) supplemented by the inner tracker (IT) surrounding the interaction region. Both subdetectors (IT and TPC) have to provide precise track finding, momentum determination, vertex reconstruction and pattern recognition.

1.2 Particles identification in the MPD

The event-by-event hadrons identification will provide us with the opportunity to measure, with high statistics, on a single event basis the yields of pions, kaons and protons, their ratios, thus giving a possibility of comprehensive study as many as possible event-by-event dynamical fluctuations and correlations. Consequently, it will provide information on possible instabilities during phase transitions, on the degree of thermal equilibrium, on collective flow phenomena and on expansion dynamics.

Physics goals of the MPD require particle identification over as large as possible phase space volume. The MPD has two main identification subsystems. The first subsystem is high performance time-of-flight (TOF) detector. The TOF together with the TPC must be able to identify charged hadrons and nuclear clusters in the broad rapidity range and up to total momentum of 3 GeV/c. The fast forward detectors (FD) will provide the TOF system with the start signal. The second PID system is the electromagnetic calorimeter. Its main goal is to identify electrons, photons and measure their energy with high precision.

1.3 Requirements for the TOF system

1.3.1 The basic requirements

Ambitious physics goals of the MPD require excellent particle identification capabilities over as large as possible phase coverage. Identification of charged hadrons (PID) at inter-mediate momenta (0.1 – 2 GeV/c) is achieved by the time-of-flight (TOF) measurements which are complemented by the energy loss (dE/dx) information from the TPC and IT detector systems.

The basic requirements for the TOF system are:

- large phase space coverage;
- high granularity to keep the overall system occupancy below 15%;
- good position resolution to provide effective matching of the TOF hits with the TPC tracks;
- high geometrical efficiency (better than 95%);
- separation of pions and kaons with up to $p_t < 1.5$ GeV/c;
- separation of (anti)protons with up to $p_t < 3$ GeV/c;
- TOF detector elements must function in a 0.5 T magnetic field.

1.3.2 The particles separation performance of the TOF

For the charged particle identification (mass reconstruction), one needs to measure the following parameters: momentum of the particle, its track length and time of flight from interaction point to the TOF detector:

$$m^2 = \frac{p^2}{c^2} \left[\left(\frac{1}{\beta} \right)^2 - 1 \right], \quad (1.1)$$

where m is the mass of the particle, p – the momentum $\beta = \frac{L}{Tc}$ is the velocity of a particle respect to the speed of light. The widths of the peaks in the mass-squared distribution depend on both momentum and time-of-flight resolutions. An analytic form [3] for the width of m^2 as a function of momentum resolution σ_p and time-of-flight resolution is determined using Eq. (1.1). The error in the pathlength L results in an effective time width that is included with the TOF resolution, σ_T ,

$$\sigma_{m^2}^2 = 4m^4 \left(\frac{\sigma_p}{p} \right) + 4p^4 \left(\frac{\sigma_t}{\beta_t} \right). \quad (1.2)$$

The momentum spectra of secondary particles at the NICA colliding energies produced in the regions of pseudorapidity $|\eta| < 1.2$ and $1.2 < |\eta| < 2$ for minimum (4 GeV) and maximum (11 GeV) colliding energies are presented in the Fig. 1.5. The average momentum of pions for energy 4 GeV is about 300 MeV/c and for 11 GeV is about 400 MeV/c.

As is known from the general theory of relativity, a particle with mass m and momentum p has a velocity:

$$\beta = \frac{p}{\sqrt{p^2 + m^2}}. \quad (1.3)$$

The time of travelling the distance L for any particle with velocity β is given by:

$$T = \frac{L}{c\beta}, \quad (1.4)$$

Using these equations, we can say that the particles separation power using time-of-flight method is determined as the number of standard deviations between time-of-flight distributions of two particles with different masses but the same momentum and track length:

$$N_{\sigma_{TOF}} = \frac{\Delta T}{\sigma_{TOF}} = \frac{L}{c\sigma_{TOF}} \left(\sqrt{1 + \frac{m_1^2}{p^2}} - \sqrt{1 + \frac{m_2^2}{p^2}} \right). \quad (1.5)$$

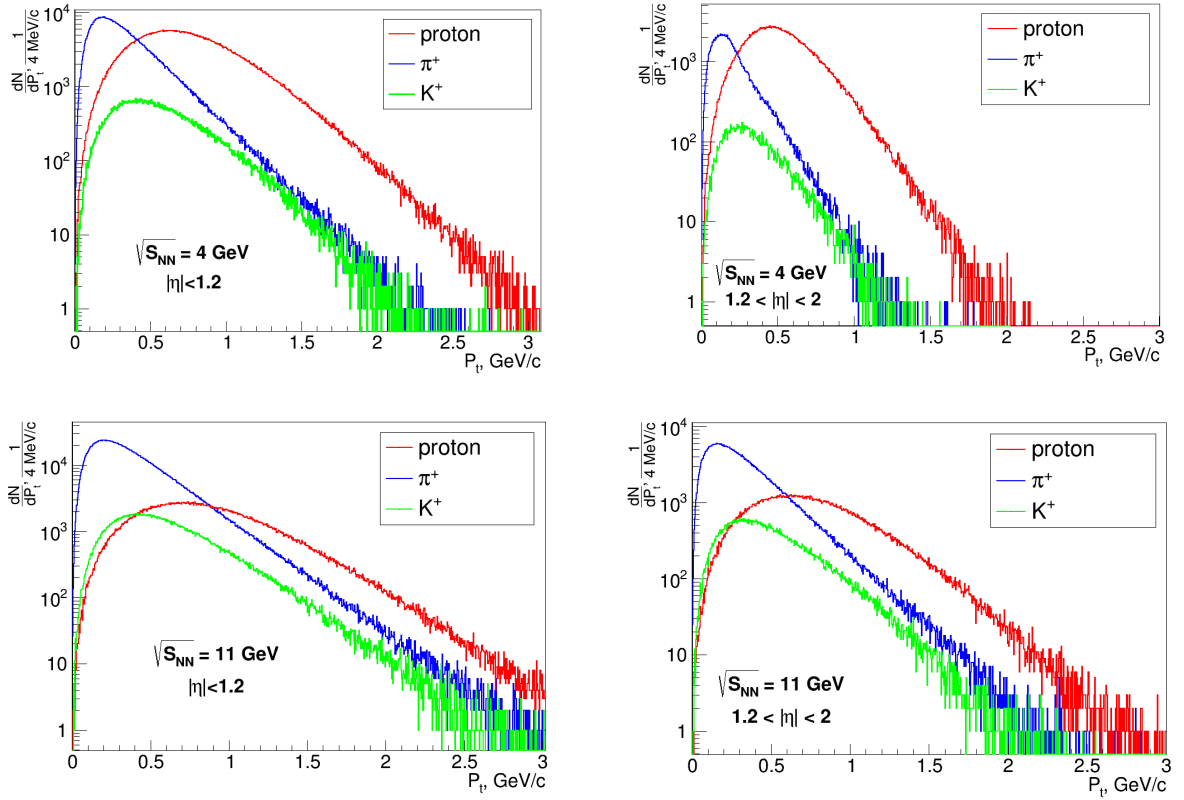


Figure 1.2: Transverse momentum spectra of pions, kaons and protons in two regions of pseudorapidity: $|\eta| < 1.2$ (left) and $1.2 < |\eta| < 2$ (right) and for two center of mass energy: 4 GeV (top) and 11 GeV (bott).

The particles separation performance could be estimated substituting the known values into the Eq. (1.2). The smallest track length for the time of flight measurement at the MPD is 1.5 m. We expect to have overall time resolution of the TOF system better than 100 ps. These conditions allow us reliable separation of pions, kaons and protons in the entire interval of momenta for produced particles for the NICA energies (Fig. 1.3a, 1.3b).

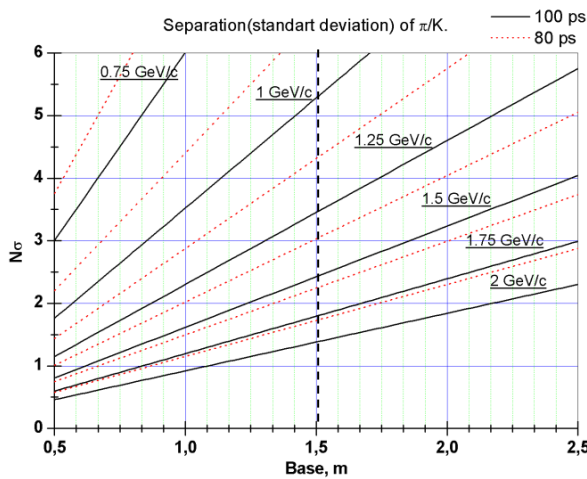


Figure 1.3a: Calculation of the separation of pions and kaons in units of standard deviation as a function of the TOF base for the TOF resolutions: 80 and 100 ps.

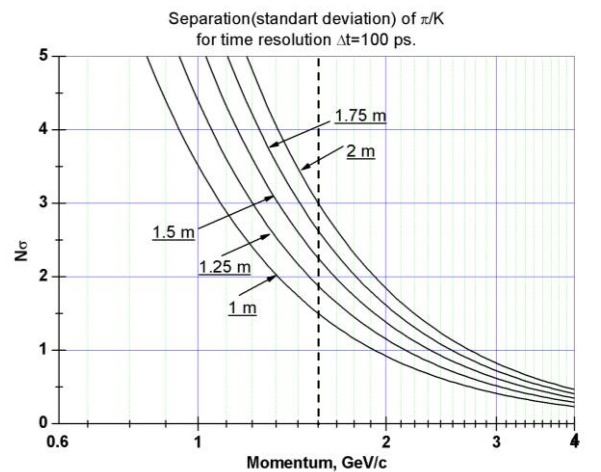


Figure 1.3b: Separation of pions and kaons as a function of secondary particles momenta for different fixed bases (time resolution is 100 ps).

In Fig. 1.4 we present the fraction (in percent) of pions and kaons below a particular momentum as a function of the momentum. These distributions are obtained for the particle spectra from Fig. 1.2. One may conclude that the TOF system can separate pions on the level of 99% and kaons – almost 98% up to the total momentum of 1.5 GeV/c.

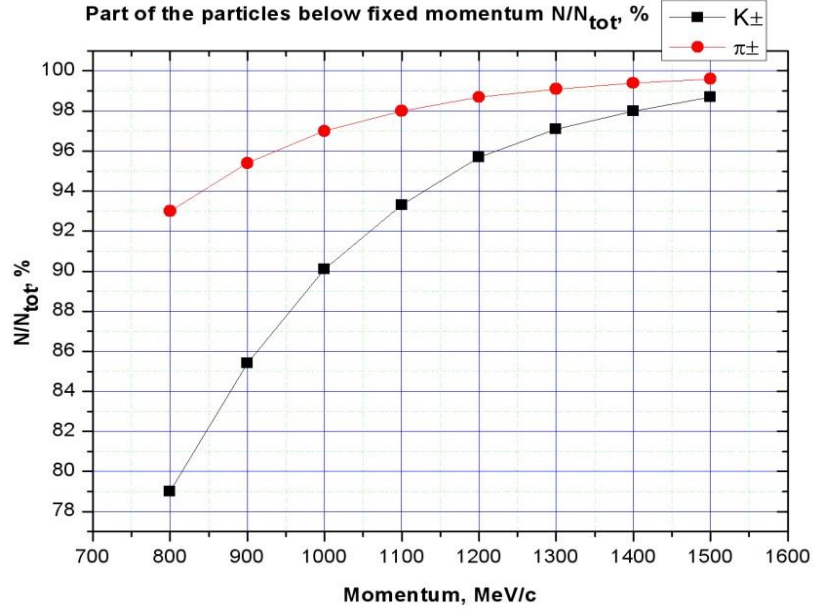


Figure 1.4: Part of the pions and kaons below a particular momentum ($\sqrt{S_{NN}} = 11$ GeV).

1.3.3 Occupancy and counting rate estimation

For simulation we used Au-Au interactions with total energy 4.5 + 4.5 GeV/n from the UrQMD generator and GEANT4 for tracing particles in the detector. Impact parameter range for minimum bias: $b = 0 - 15.8$ fm, for central collision: $b = 0 - 3$ fm.

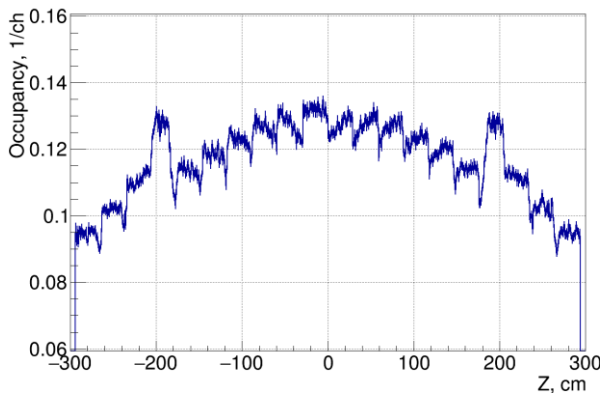


Figure 1.5: Estimated mean occupancy of the TOF system as a function of Z per one central Au-Au event with energy of 11 GeV.

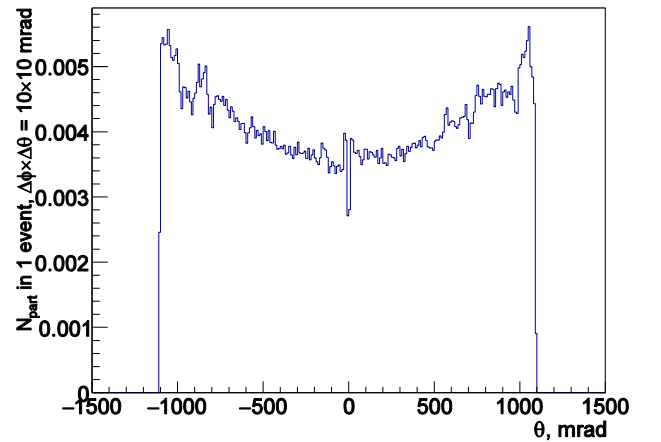


Figure 1.6: Charged particles multiplicity per one minimum bias interaction as a function of $(\theta-\pi/2)$.

Simulated occupancy of the proposed TOF system for all charged particles is shown in Fig .1.5. Maximum occupancy does not exceed 14% per channel in the barrel even considering secondary particles and cross-talks on the strips.

For particles rate estimation the anticipated luminosity for Au + Au collisions $L = 10^{27} \text{ cm}^{-2}\text{s}^{-1}$ was used. The collision rate for minimum bias events was taken as:

$$L \times \sigma = 1 \cdot 10^{27} \times 6 \text{ barn} = 1 \cdot 10^{27} \times 6 \cdot 10^{-24} = 6000 \text{ Hz}$$

The interaction rate for central collisions is below 1 kHz. From Fig. 1.6 one can see that there are 0.005 charged particles that cross the surface of 2.6 cm^2 in one event. The number of charged particles per second crossed the 1 cm^2 surface of the TOF is only $N = 6000 \text{ Hz} \times 0.005 / 2.6 = 11.5 \text{ Hz/cm}^2$. Our rate test of the MRPC prototype on the extracted beam of the Nuclotron demonstrated a good timing performance and its efficient work at particle fluxes up to $10^3 \text{ cm}^{-2}\text{s}^{-1}$ (see Fig. 2.15). Thus, the TOF MPD system based on the MRPC has to demonstrate reliable work at particle flux bellow 12 Hz/cm^2 .

2 Development of the MRPC for the TOF

2.1 Motivation of choosing the MRPC for the TOF system

Our choice for the TOF system is the Multigap Resistive Plate Chambers (MRPC), which were widely used in such heavy-ion experiments as ALICE [4, 5], PHENIX [6], STAR [7], HADES [8] and is planning the TOF CBM [9]. Such widespread use of this detector caused by that the multigap resistive plate chamber has good timing characteristics. At the same time, the MRPC is quite easy to manufacture and it is relatively inexpensive. Its production requires materials that are commercially available.

The multigap resistive plate chamber consists of a stack of resistive plates separated one from the other with equal size spacers creating a series of gas gaps [10]. High voltage coating is made on the outer surfaces of the outer resistive electrodes. Internal plates are left electrically floating. The voltage of the internal plates appears due to the flow of electrons and ions created in the gas gap. The resistive electrodes quench the streamer and prevent a spark breakdown. The MRPC operates at high gain in avalanche mode. Float glass plates are used as resistive plate electrodes.

2.2 Designs of the MRPC prototypes

Two types of MRPCs were considered: with the pad signal readout and with the strip readout. Both options have their special traits in terms of assembling and operation. However, at low multiplicity of events, it makes sense to use a strip electrode for readout. It reduces the number of channels making the system more cost-effective. Therefore, strip MRPCs have been chosen for the barrel part of the MPD. At the end cup parts of the detector, pad and strip readouts will be combined there.

The first prototype of a multigap resistive plate chamber (MRPC) for the TOF MPD (Fig. 2.1) was made small with pad readout [11]. A 208 μm gas gap is formed by a monofilament fishing line of appropriate thickness. The readout electrodes are PCB of $140 \times 120 \text{ cm}^2$ with copper rectangles of $16 \times 35 \text{ cm}^2$. In total they make up two rows of 8 pads in each. In order to supply high voltage to glasses closest to the readout electrodes, they are coated with a graphite conductive layer with a surface resistance of 2 – 10 $\text{M}\Omega$ per square. Signals from the pads are transferred via the twisted pair cable to the amplifier. The detector is situated in a leak-tight box (Fig. 2.2) in which a gas mixture is injected.

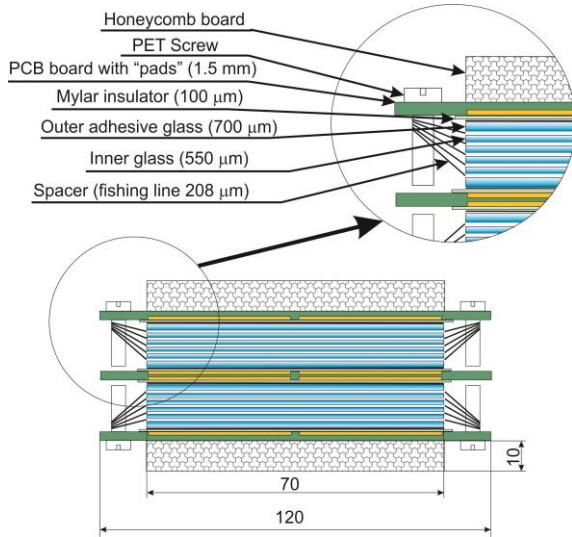


Figure 2.1: Pad MRPC scheme.

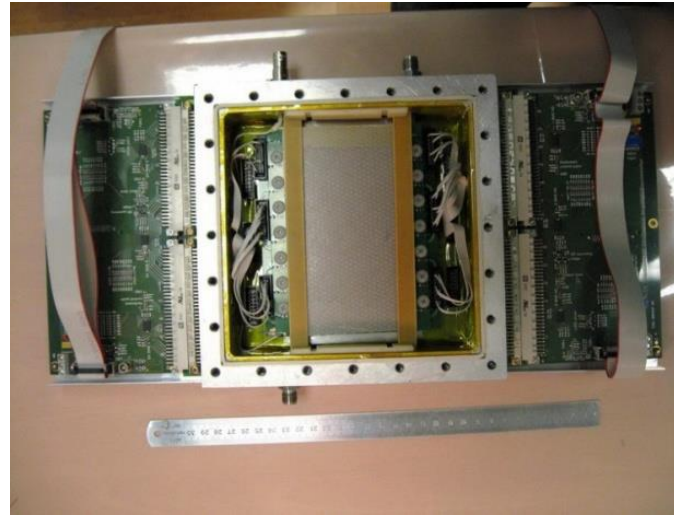


Figure 2.2: Pad MRPC prototype in gas box.

The expected multiplicity of particles in the central Au + Au collisions at $\sqrt{s_{NN}} = 11$ GeV allows using readout electrode area of 100 cm^2 with the maximum occupancy about 25%. On the other hand, increasing the size of the electrode can lead to time resolution worsening due to the signal deterioration (front drops). In case of using readout electrode as a long narrow strip and reading signal from both sides, it avoids the need to take the time dependence of the position of the flight of the particle into account. This method significantly reduces the number of channels of readout electronics without degrading the time resolution.

The last and more successful strip prototype with an active area of $600 \times 300 \text{ mm}^2$ has been designed and tested on the beam. Main features of this MRPC are three stacks [12] of glass and the readout from the inner stack (Fig. 2.3). In order to get good time resolution from MRPC by using the time-over-threshold method one needs to provide very good termination of impedance between the strip, the cable and the preamplifier input. Any reflection could cause the wrong estimation of the signal width when the amplitude correction applied. Working with double stack MRPC with differential signal readout scheme one also has to pay attention to the fact that readout strips for positive and negative signals have different impedances. The inner strip is surrounded on both sides by the fiberglass PCB and glass with dielectric constant ~ 4 . The external electrodes have a honeycomb on one side and glass from the other. As a result, the positive and negative parts of the signal propagate with different velocities. This fact can lead to worsening of time resolution. One can make the impedance of anode and cathode strips in the double stack MRPC equal by introducing the honeycomb spacer between two inner PCBs. A single-stack MRPC is the example of good electrical symmetry. However, getting a large signal often requires more than 6 gaps. Large number of gaps reduces capacitance of the strip line. A proposed triple-stack MRPC design is free of the mentioned above problems.

Each stack of the detector consists of 5 gas gaps width of 200 μm separated by the thin (280 μm) glass. Such thickness of the glass was chosen for two reasons. Firstly, it reduces the radiation length of the detector, and secondly, it improves the rate capability of the detector [13]. The active area of the MRPC is determined by the size of the glass (300×600 mm). Signals are read from two sides of 24 readout strips 10 mm wide using the double twisted pair flat cable (Fig. 2.4).

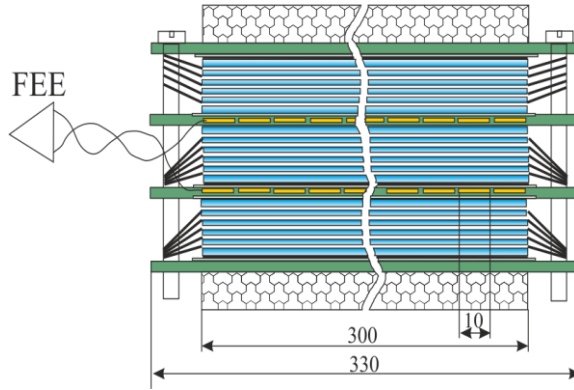


Figure 2.3: Layout of the strip MRPC.



Figure 2.4: Readout from three stacks of the MRPC.

2.3 Beam setup and cosmic stand for testing detectors

The principal goal of the R&D is to investigate the problems associated with scaling up from a small to a full size MRPC with strip readout electrodes. Various issues were addressed, such as: (a) material and thickness of resistive plates (b) definition of the edge of the active area (c) connection between readout electrodes and electronics (d) assembly problems and (e) front-end electronics. The tests were performed in both cosmic rays and proton beam of the Nuclotron.

Laboratory with cosmic test setup was organized (Fig. 2.5) for testing detectors in the intervals between runs of the Nuclotron. Cosmic stand includes (Fig. 2.6): scintillation telescope (S1-S8) which cover the entire active area of the tested detectors; 4-channel gas system with MKS-Instruments controllers; fast readout electronics based on VME (ADC, TDC, TQDC ...); high-voltage and low-voltage power supplies; the oscilloscope LeCroy Wave Runner with a bandwidth of 4 GHz; x-ray tube; fast start detector (FFD); slow control system (temperature, gas flow, currents and voltages of the high and low voltage power supply).



Figure 2.5: Appearance of the cosmic test setup.

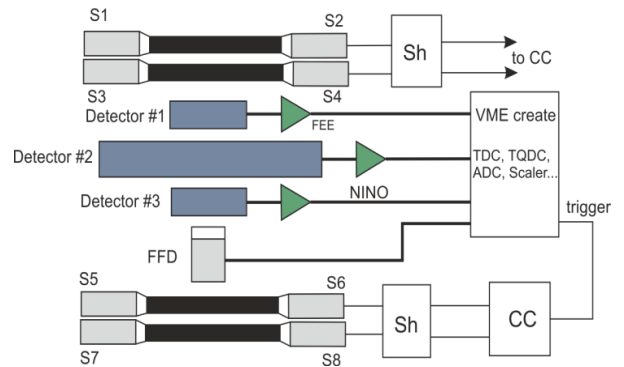


Figure 2.6: Diagram of the cosmic test setup.

“Test beam MPD” facility [14] is a complete system of equipment and devices for studying detectors on the beams of particles (deuterons) from Nuclotron with energy range 1 – 4 GeV/n.

It includes (Fig. 2.7):

- two platforms made of aluminum profile for fixing and adjustment detectors along a beam axis;
- the precision positioning device for movement and turn of the tested detector concerning a beam axis operated by remote control;
- three proportional chambers (MWPC 1, 2, 3) with 6 coordinate planes for tracking and definition of the profile of the beam with an accuracy of determination of coordinate about 1 mm;
- five scintillation counters for trigger and to determine the intensity of the beam;
- gas system consisting of two independent control panels, allowing to prepare the gas mixture to blowing various gas-filled detectors with different gas mixtures (MRPC, GEM, DC etc.);
- data acquisition system (DAQ) based on the standard VME and Ethernet, allowing to control operation of the detector "on-line", as well as to record data files for further processing.

The beam room and control room are provided with temperature stabilization system.

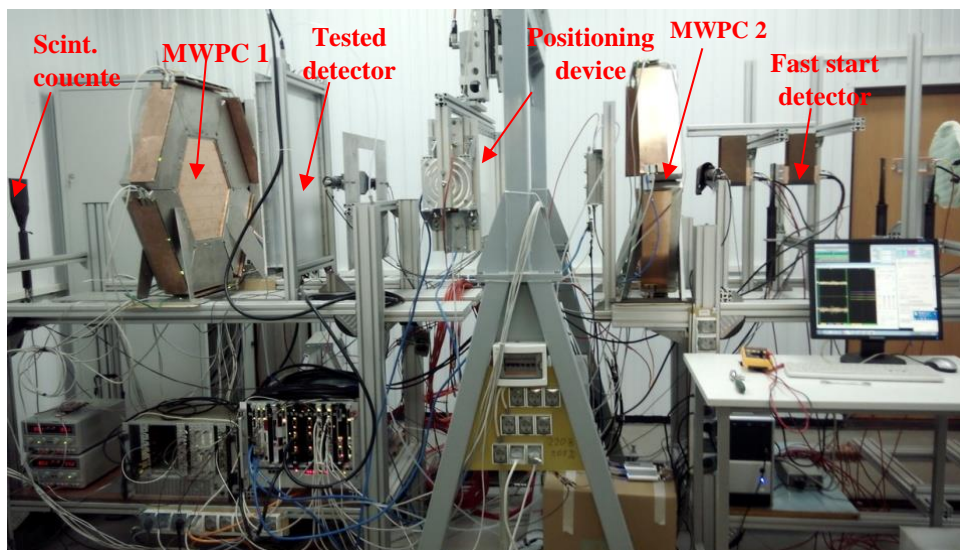


Figure 2.7: General view of the “Test beam MPD” setup during working in the 51 Nuclotron run.

2.4 Test results

Detectors were tested on deuteron beam of the Nuclotron with energy of 3.5 GeV/nucleon. The start signal to define the time of flight was generated by the fast Cherenkov detector with micro-channel photomultiplier Photonis Planacon XP85012Q. The time resolution of the “start” detector is about 37 ps [15].

The total time resolution of the system FFD-Pad MRPC was approximately 70 ps (Fig. 2.8). Thus, the time resolution of the pad MRPC prototype was in the region of 60 ps (including the “jitter” of electronics) the with particle detection efficiency of about 99% (Fig. 2.9).

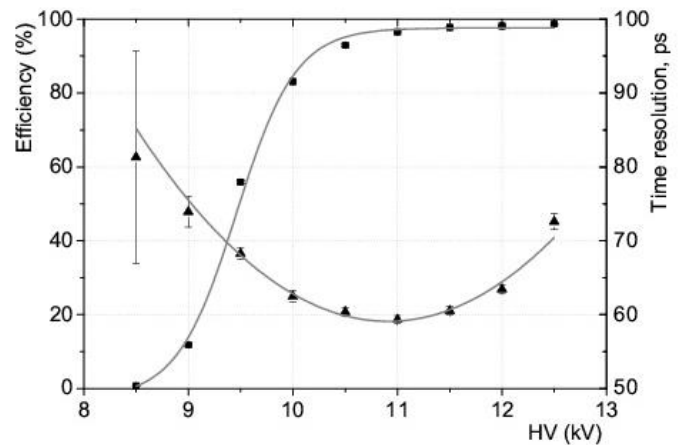
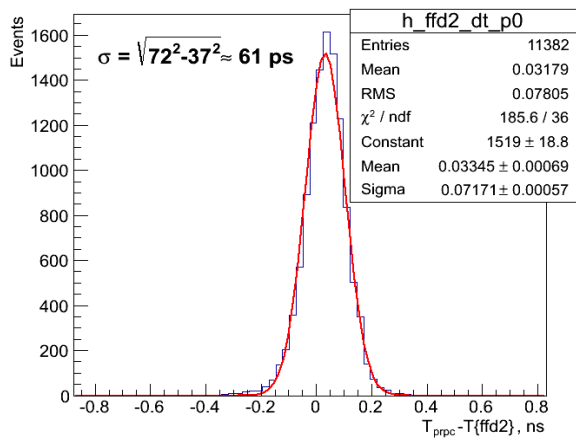


Figure 2.8: The distribution of the difference between the start detector and the "pad" MRPC. **Figure 2.9:** Efficiency and time resolution of the "pad" MRPC in dependence of high voltage.

Dependence of the efficiency and time resolution for strip MRPC from applied high voltage is shown in Fig. 2.10. Efficiency, due to the large number of gas gaps, quickly reaches a plateau of 99.5 %. The best time resolution (~ 42 ps) is observed at approximately 12 kV [16].

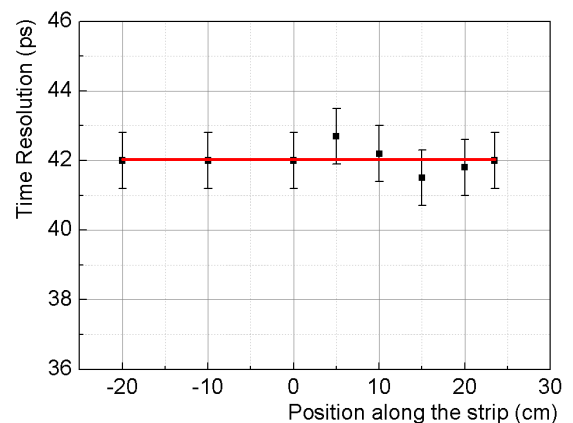
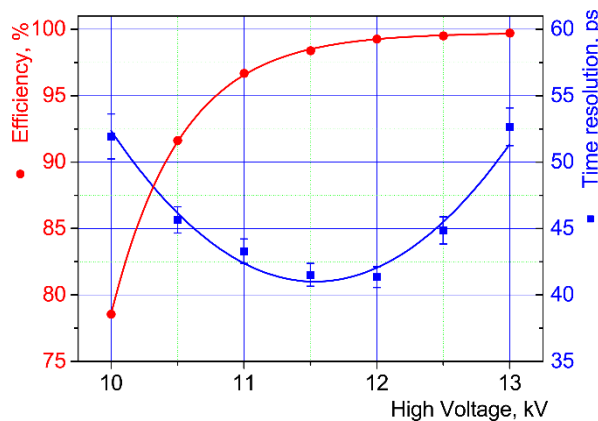


Figure 2.10: Efficiency and time resolution of the strip MRPC versus high voltage. **Figure 2.11:** Time resolution in dependence from position along the strip.

Upon further increasing of the high voltage the number of streamers rises sharply and the resolution degrades. The time resolution of the detector does not change due the position of the particles tracks along the strip (Fig. 2.11). All time resolution results include jitter of electronics which is about 20ps.

Particles crosses detector at different angles in a real experiment. Angle between the particle tracks and the plane of the detector can reach 60 degrees on the edge of the barrel. Measurements of parameters of the detector from the angle of passing of particles were made (Fig. 2.12). The efficiency not changes at angles from 0 to 60 degrees. The time resolution varies slightly, but overall <52 ps. Mean number of fired strips at angle of 0 degree is 1.28 (Fig. 2.13). The cluster size goes up with increasing of angle. Increasing of strip multiplicity determine by two factors. First factor is distribution of the charge for a few strips. Second factor is increase of projection of track along the detector.

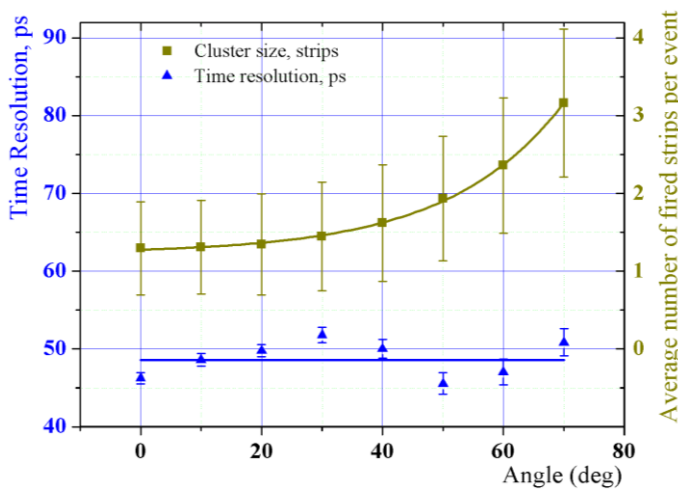


Figure 2.12: Time resolution in dependence of MRPC rotation in surface YZ (across the strip).

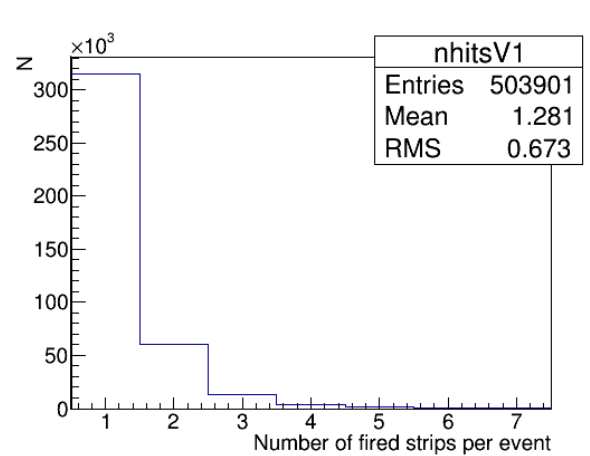


Figure 2.13: Distribution of the number of fired strips per event for particles with zero angle.

2.5 Study of rate capabilities of a MRPC

In order to use MRPCs in endcap TOF one need to keep in mind high multiplicity of particles (up to 2000 particles/(cm²·s)) expected in the regions close to the beam axis for the peripheral events. It is known that MRPC made of ordinary glass with thickness of 400 microns are effective at particles rates up to 1 kHz/cm². Therefore it is necessary to have detectors operating at high particles intensities. Two case of solving the problem were chosen: reducing the thickness of the glass [13] and reducing its conductivity [17].

High rate MRPCs made of low-resistance "Chinese" glass were tested on the beam of high intensity in the 47 run of Nuclotron with a group of physicists from the Tsinghua University

(Beijing, China). Prototype with a low resistance glass showed excellent rate capability, as expected. Its efficiency was higher than 90 % at particles rates up to 100 kHz/cm². At the same time resolution was better than 80 ps. The time resolution of this MRPC reached 52 ps (Fig. 2.14) at low fluxes of particles.

The high rate test of MRPC made on thin float glass took place during the 50 run of Nuclotron [16]. Two prototypes of MRPCs were tested. Both MRPCs have identical construction but first of them made on glass with thicknes 270 mkm, and second prototype made on glass with thicknes 400 mkm. Degradation of efficiency and time resolution are showed on Fig.2.15. Prototypes with different thin ordinary glass could be used in area where the particle flux will be less than 2 kHz/cm².

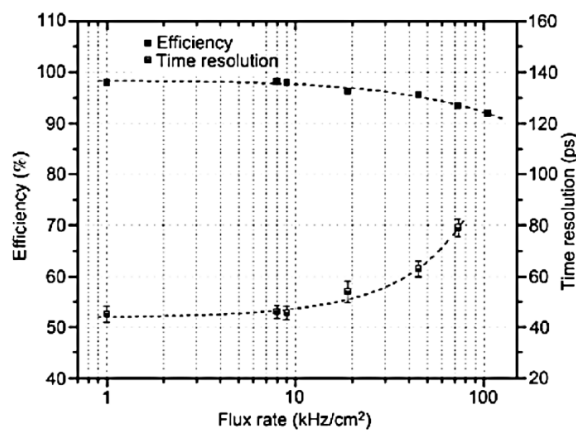


Figure 2.14: Efficiency and time resolution of MRPC with low-resistance glass from the beam intensity.

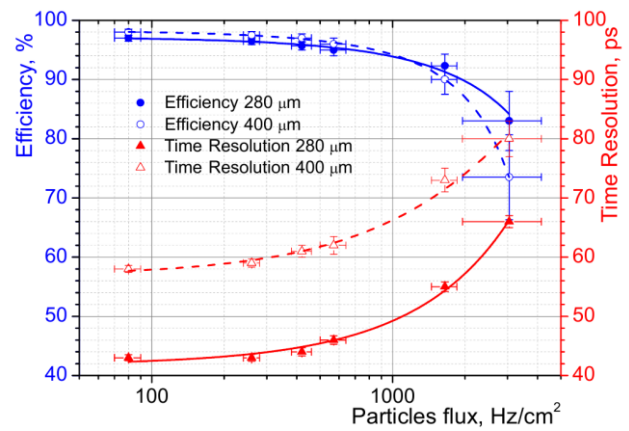


Figure 2.15: Efficiencies and time resolution of MRPCs with different glasses from the beam intensity.

3 The MPD TOF system design

3.1 Detail layout of the MRPC for the MPD time-of-flight system.

After analyzing the results of the prototypes testing, we have fixed the design and geometry of the MRPC for the TOF barrel. It will be triple stack MRPC with strip readout.

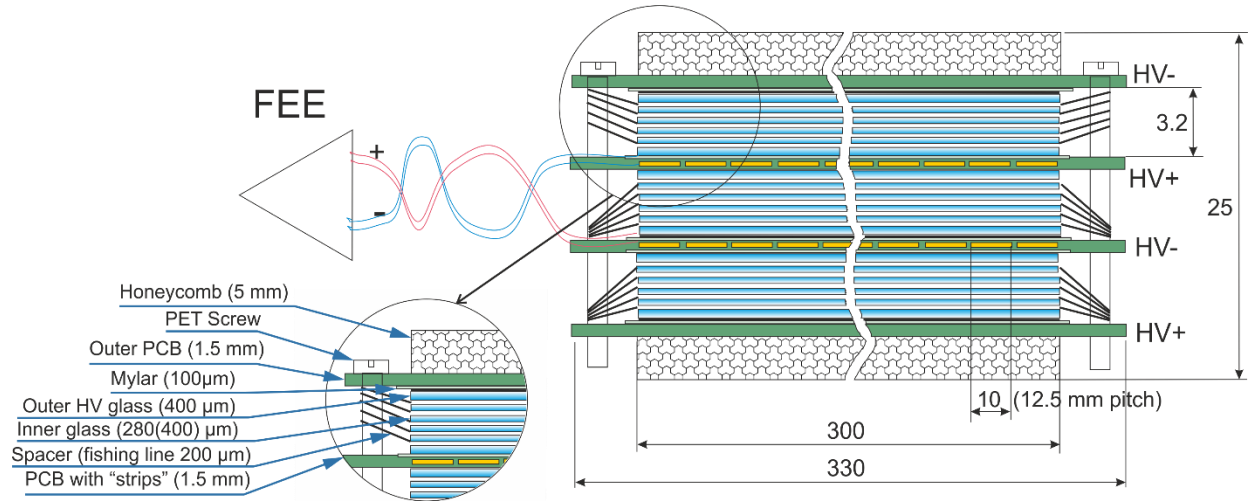


Figure 3.1: Scheme of the triple-stack MRPC with strip readout for TOF MPD.

A scheme of the MPD TOF detector is presented in Fig. 3.1. The detector consists of three stacks of 5 gas gaps each. As resistive electrodes we use common float glass. The outer glass electrodes have the thickness of 0.4 mm. The internal glass electrodes have the thickness of 0.270 mm. The fishing line as a spacer defines the 200 μm gap between the all resistive electrodes. The outer part of external glass electrodes is covered by the conductive paint with surface resistivity about 2 – 10 $\text{M}\Omega/\square$ to apply high voltage. All internal glasses are floating. Dimensions of the resistive glass are 300 x 640 mm^2 . It defines a surface of active area of one MRPC.

An important feature of the triple-stack “strip” prototype is that readout strips are located only inside of the detector. Outer PCBs are not metalized. This ensures the symmetry between two strips, and provides the equal speed of signals on the anode and cathode strips and as a result prevents the dispersion of the signal.

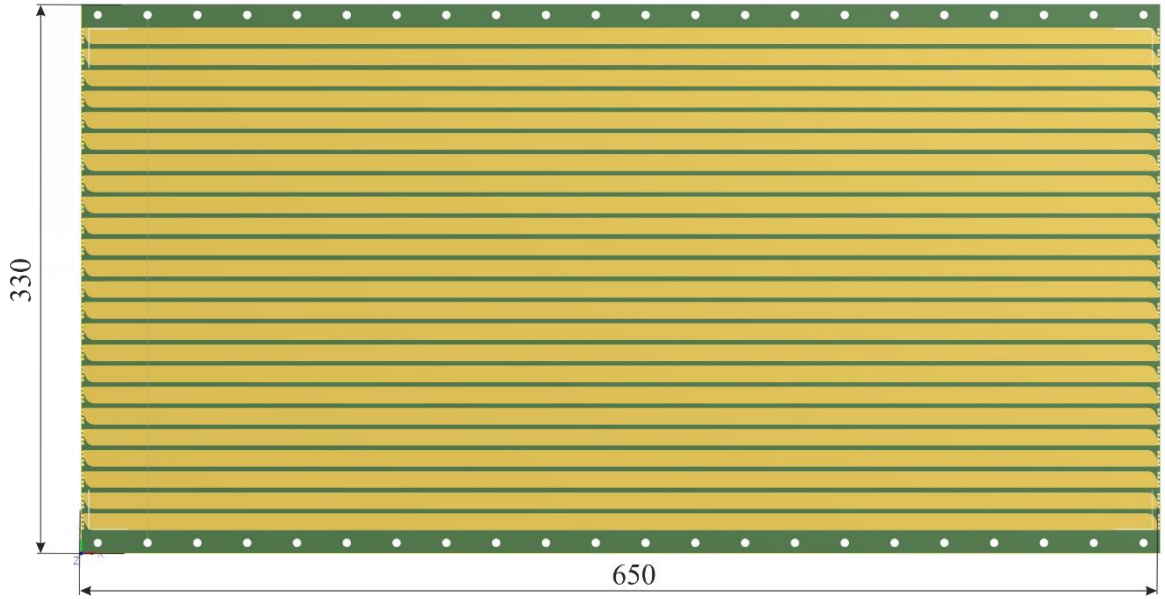


Figure 3.2: Readout PCB with 24 strips 10 mm wide.

Overall dimensions of the MRPC are $650 \times 330 \times 25 \text{ mm}^3$ and it corresponds to the PCB with readout electrodes (Fig. 3.2). PCB has 24 strips, 10 mm wide and 640 mm long. To reduce crosstalk, the gap between strips is 2.5 mm. Thus, the pitch of electrodes in this case is 12.5 mm. The active surface of one strip is about 80 cm^2 . Mean occupancy for this area (see Fig. 1.8) should not exceed 15% for central Au-Au collisions with energy $\sqrt{s_{NN}} = 11 \text{ GeV}$.

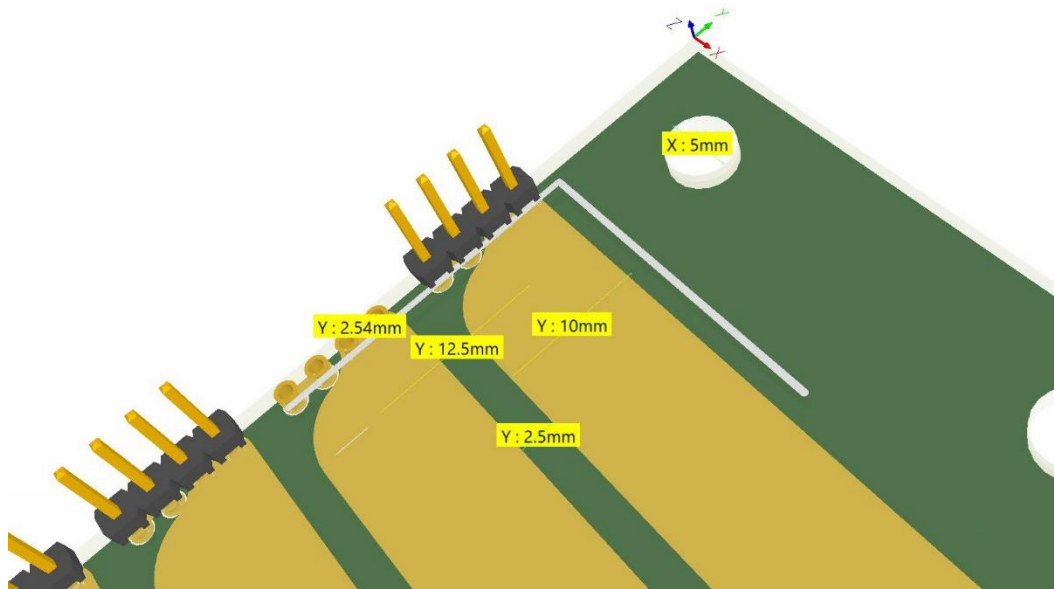


Figure 3.3: PLH pin connector on the one strip of the PCB.

The pickup electrodes made at the inner layer of the PCB. It is necessary for better electrical isolation of strips from high voltage layer. The signals are output to the outer layer of the anode and cathode boards in such a way that the differential signal is read through one PLH pin connector (Fig. 3.3) that combines both boards.

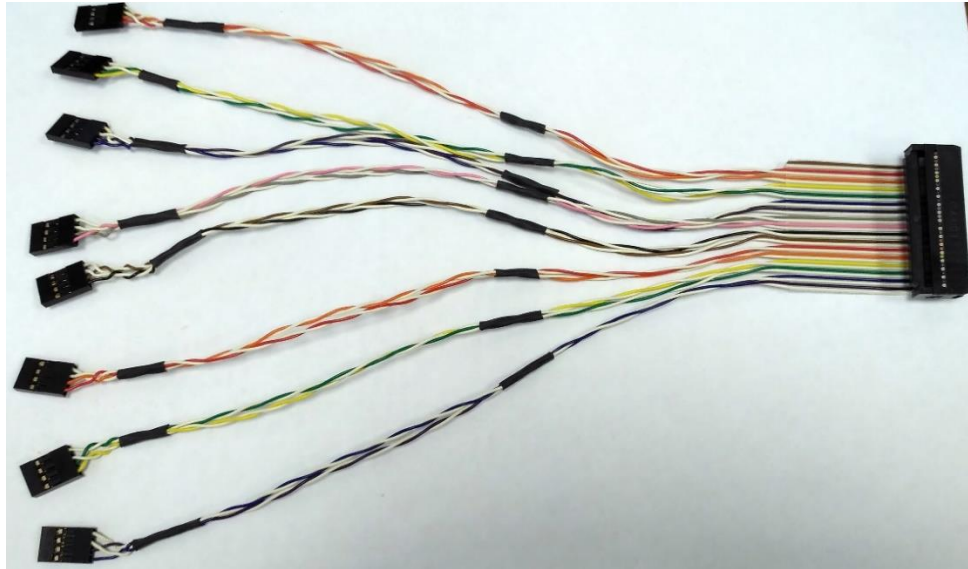


Figure 3.4: Dual twisted pair cable assembly for transferring signals to the FEE.

The differential analog signal is transferred from both ends of the strip by the doubled twisted pair cable (Fig. 3.4) with impedance of 55 Ohm to the front-end electronics. Double-side readout provides better time resolution and determination of the coordinate of a particle along the strip with spatial resolution of ~ 5 mm. For stiffening structure, we glue aramid fiber honeycomb panel with the thickness of 5 mm on the outer part of the external PCBs. The first prototypes of MRPCs (Fig. 3.5) for the TOF MPD already assembled and tested.

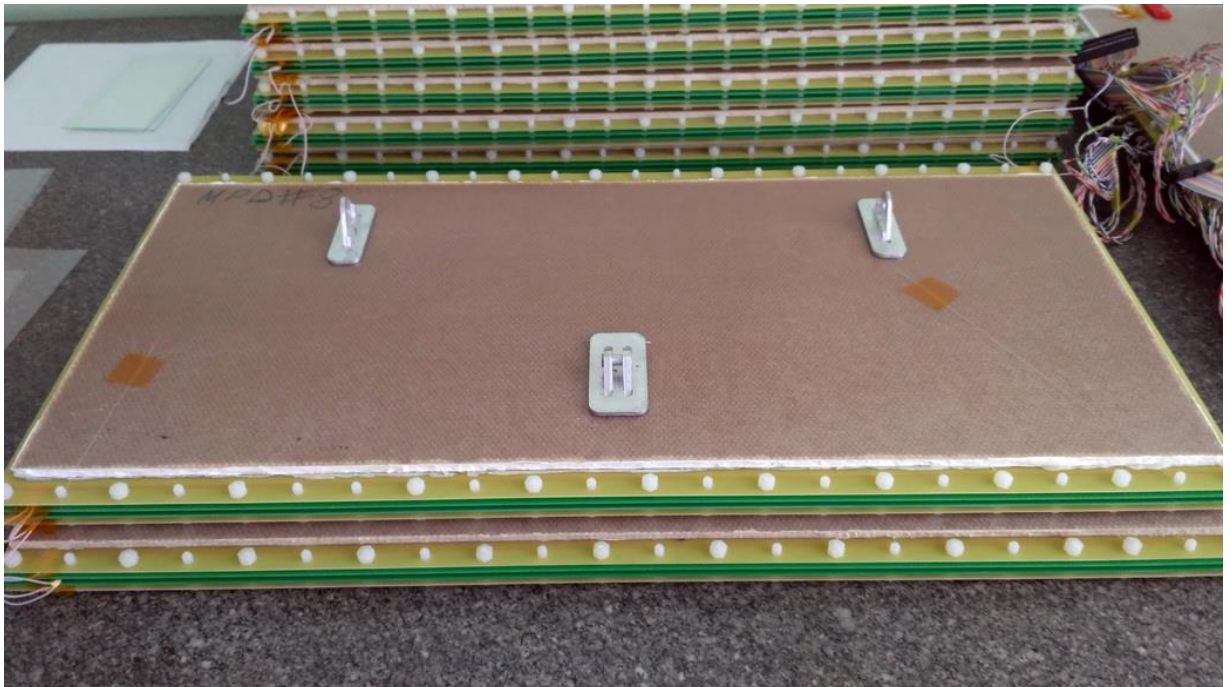


Figure 3.5: First assembled MRPCs for the MPD TOF system.

3.2 Mechanical design of the TOF barrel

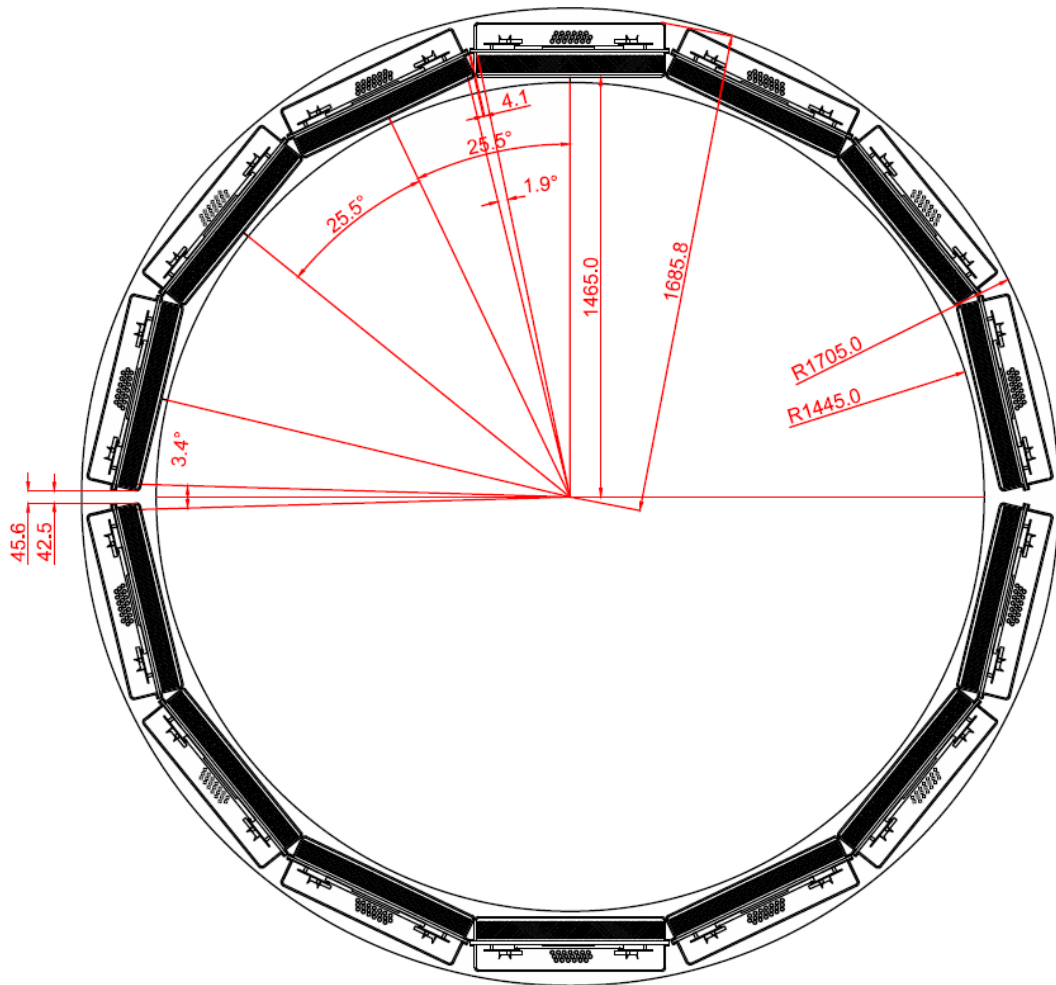


Figure 3.6: Main sizes of the TOF barrel in ϕ direction.

The cylindrical part of the TOF MPD is located in the barrel between the time-projection chamber (TPC) and the electromagnetic calorimeter (ECal). The TOF barrel internal radius is about 1.5 m from the beam axis and outer radius is 1.7 m (Fig. 3.6). The active surface of the barrel part of the MPD ToF covers the pseudorapidity range $|\eta| \leq 1.4$ and $\sim 330^\circ$ in ϕ angle. The total surface of the barrel TOF system is about 52 m². The TOF detector system is organized in a modular way in order to minimize the number of components and cost.

The detector is segmented in ϕ direction into 14 pairs of modules of ~ 5.9 m length. The maximum distance between two boxes does not exceed 5 mm. The special shape of module minimizes the dead area inside the sector. The dead area between modules along ϕ direction is due to the limited space along the radius of barrel. This fact does not allow putting modules with overlap azimuthally dire. Wide gaps in the horizontal plane are required for support structures for mounting the TPC.

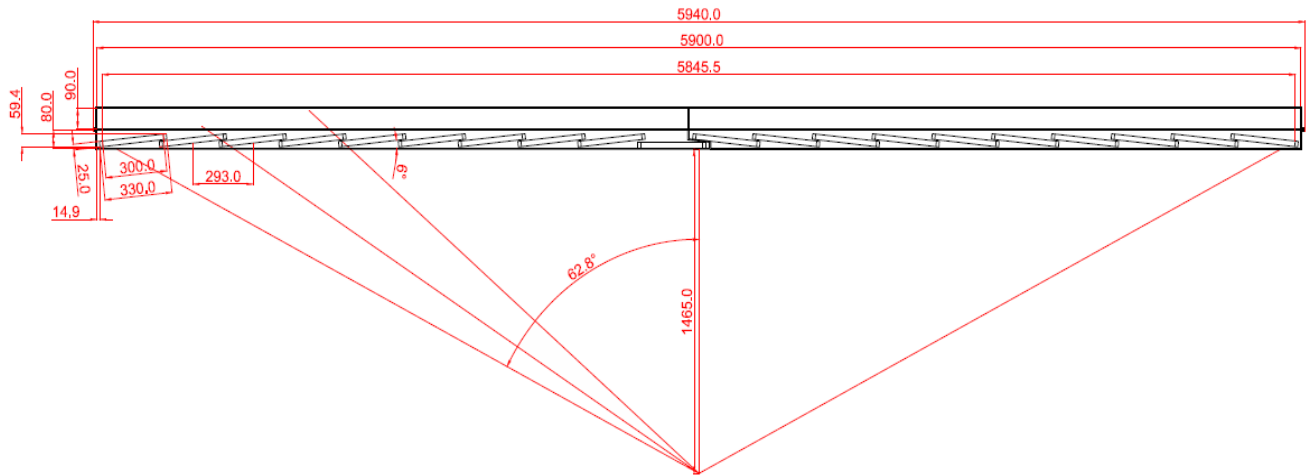


Figure 3.7: Arrangement of MRPCs inside the gas boxes along the beam direction.

Each TOF module consists of a two separate volumes. The inner region is filled of the gas mixture and contains 10 MRPCs. The outer one contains the Front End Electronic (FEE) cards, cables, high voltage and gas plugs. The both boxes are made of the aluminum profile and honeycomb 5 mm thick. The same honeycomb panel with thickness of 10 mm is located between inner and outer volumes. It has special holes for the Interface Card (IC), which provides connection of signals from MRPCs to preamplifiers. Holes for gas connectors and the HV connectors are also provided at this panel. MRPCs are arranged inside the box as shown in Fig. 3.7. Special aluminum fixators (Fig. 3.8) are used to set detectors to the desired position.

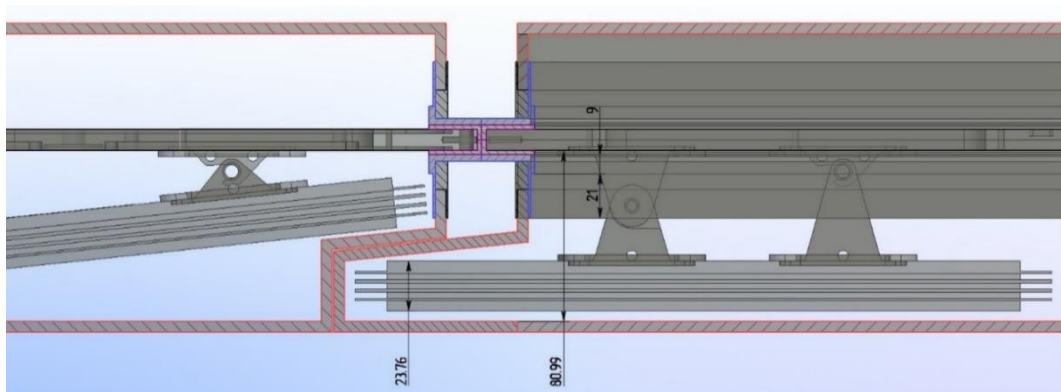


Figure 3.8: Fixing of MRPCs inside the gas box using special elements.

Adjacent MRPCs will be positioned inside the module in such a way as to create an overlap of 1-2 readout strips between two adjacent MRPCs, at the edge of the active area: this will ensure the inter-calibration of the MRPCs via tracks traversing both of them. The signals from the pick-up strips on the MRPCs are brought to the front-end electronics (FEE) via the Interface Cards. The ICs are made of small PCBs and will be glued and fixed to the top cover of the box closing the gas volume in this way. Each IC will have on one side the connectors facing the MRPC, and the connectors for the FEEs on the other side. To add safety to the system the perimeter of the IC is poured with epoxy adhesive.

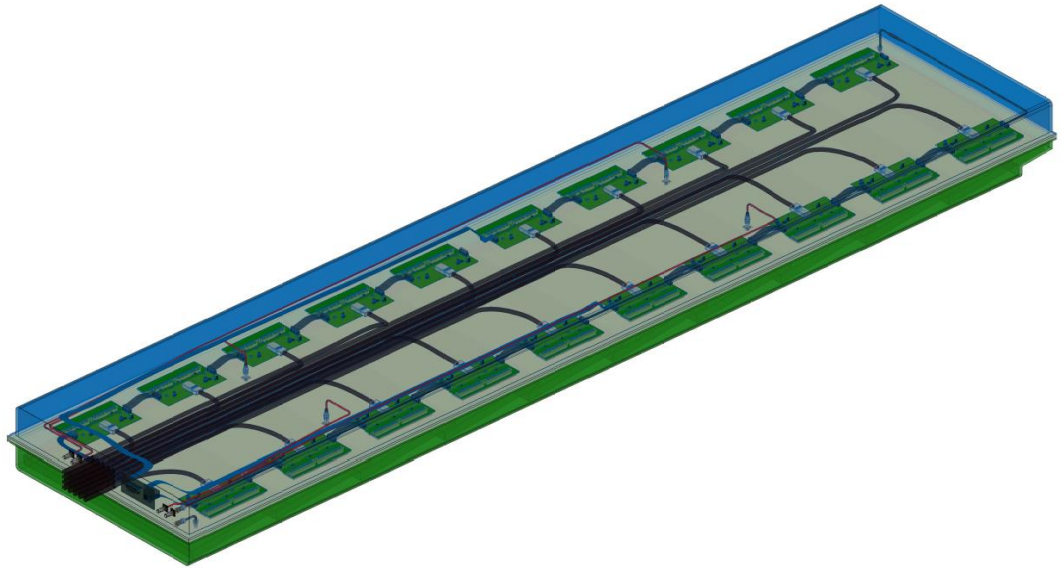


Figure 3.9: Layout of FEE, cables and connectors inside the module.

The volume containing front-end electronics and cables is enclosed within a same aluminum honeycomb cover like for the gas volume. Cables taking the signals from the FEE, LV cables, gas tubes and slow control buses will be routed through the center of the module to its outer ends (Fig 3.9). Then they will come out from the external sides of the sector and pass through special holes in the yoke. Total surface of one hole is about 690 cm^2 . Crates with readout TDCs planned to mount directly on the MPD magnet yoke (Fig 3.10) opposite both ends of the barrel TOF. The space about 30 cm^2 ($< 5\%$ of total size) is enough in each hole in the yoke for all cables, tubes. Signal cables with a diameter $\sim 13 \text{ mm}$ require the most space ($\sim 23 \text{ cm}^2$) for output.

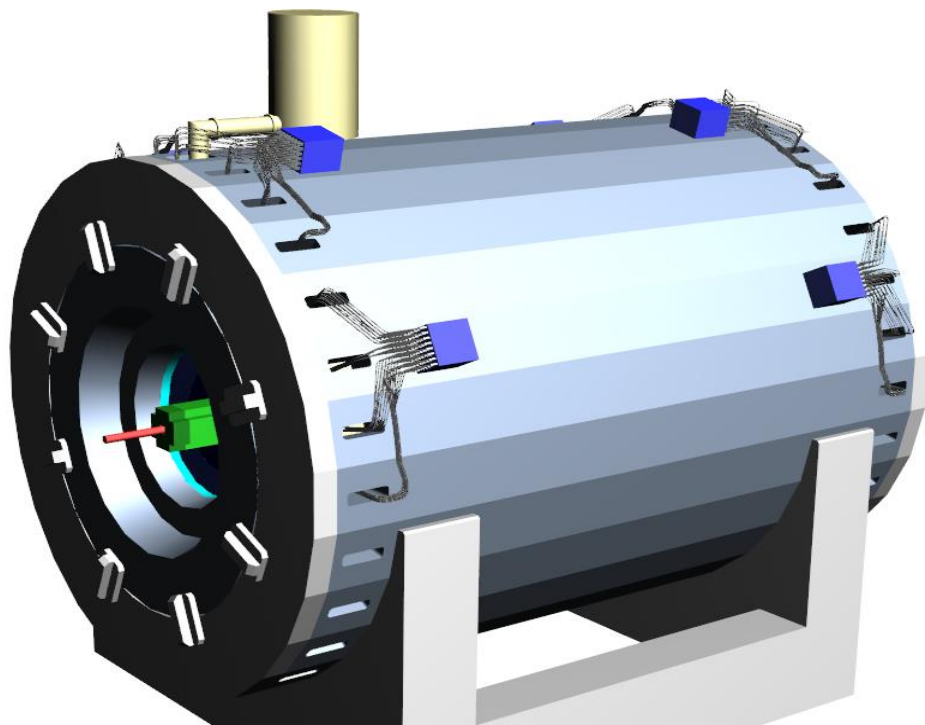


Figure 3.10: Crates with readout electronics are mounted on the magnet yoke.

Main parameters of the TOF system parts are listed in Table 3.1. Calculated total sensitive area of the TOF system is about 51.8 m². The inner radius of the barrel is about 1.5 m. The total area of a barrel with this inner radius and length of 5.9 m is about 55 m². This means estimated geometrical efficiency should be about 94%.

Table 3.1 Main parameters of the TOF system.

	Number of detectors	Number of readout strips	Sensitive area, m ²	Number of FEE cards	Number of FEE channels
MRPC	1	24	0.192	2	48
Module	10	240	1.848	20	480
Barrel	280	6720	51.8	560	13440 (1680 chips)

3.3 The occupancy and geometric efficiency of the TOF system.

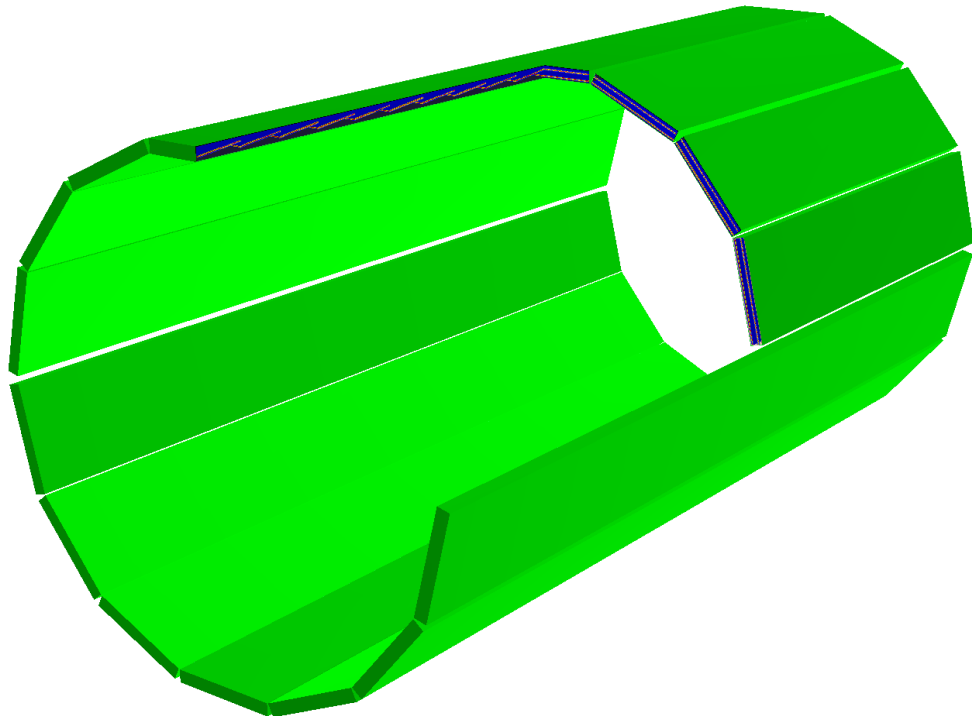


Figure 3.11: The TOF detector layout in the MPDROOT framework.

Monte Carlo simulation has been performed using the MPDROOT framework based on the CERN ROOT software. The MPDROOT framework has interfaces to several event generators (UrQMD, QGSM, HIJING, etc.) and includes all algorithms for MPD reconstruction and analysis, thus providing a complete set of instruments to simulate ion-ion collisions. The barrel of the MPD TOF system is a cylinder covering the region of polar angles $|\theta - 90^\circ| < 63^\circ$ ($|\eta| < 1.4$). The structure of the TOF, the inner structure of each module and MRPC detectors have been described in the GEANT 4 package. All simulations have been done for geometry presented in the previous chapter. The three-dimensional model of the TOF is shown in Fig. 3.11.

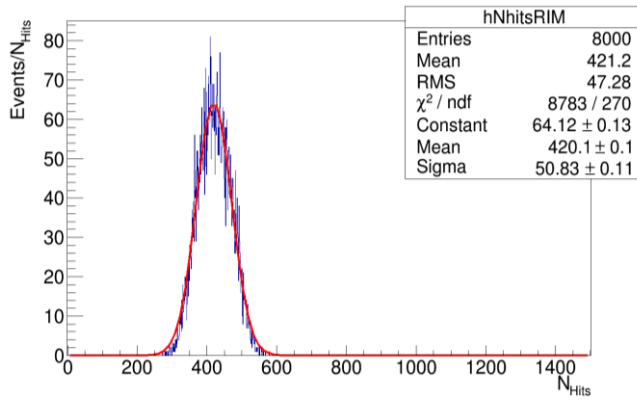


Figure 3.12: Multiplicity of primary particles (from generator) registered by the TOF system in Au-Au collision with energy of 11 GeV.

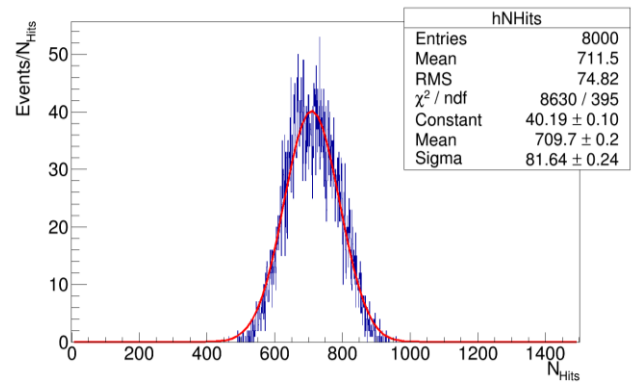


Figure 3.13: Multiplicity of all particles (primary, secondary, delta-e, conversion) registered by the TOF system in Au-Au collision with energy of 11 GeV.

Preliminary results of the simulation showed that such geometry of detectors and readout electrodes satisfies the requirements of the experiment.

The procedure of calculation of occupancy is as follow. We calculate the number of hits (taking into account the experimental data for cluster size in dependence on the particle input angle Fig. 2.13) from all MC tracks in central (0-3 fm) collision of Au-Au with maximum NICA energy $\sqrt{S_{NN}} = 11$ GeV. As a result, we can get a distribution of the number of fired strips in the TOF. We obtained the distribution presented in the Fig. 3.12 for the primary tracks. It can be seen that for primary tracks the mean occupancy is only $420/6720=6.25\%$. The distribution for all registered in the TOF particles is in the Fig. 3.12. From this distribution can be obtained the maximum expected occupancy: $900/6720=13.4\%$ (Mean occupancy in this distribution is $\sim 10.5\%$). Thus, the contribution of secondary particles is quite significant.

The geometrical efficiency depends on the geometry of whole TOF system and arrangement of the MRPCs in the TOF. The efficiency in Fig. 3.14 is differential efficiency ($d\epsilon/dZ$) along the Z direction with step of 1 cm and averaged over the angle φ (sum of particles for all 14 modules/14). The same distribution along φ direction averaged over the beam direction is presented in Fig. 3.15.

It follows from the Fig. 3.14 and Fig. 3.15 that 93,5% of all particles flying in direction of the TOF fall into the active region of detectors. The others (inefficient) fly through the gaps between the modules.

The origin of the zigzags in the efficiency can be explained as follows. The upper zigzag peak corresponds to the lower edge of the detector in adjacent modules. In this position, the active regions of adjacent modules are closest to each other. Therefore, more particles are recorded at this location.

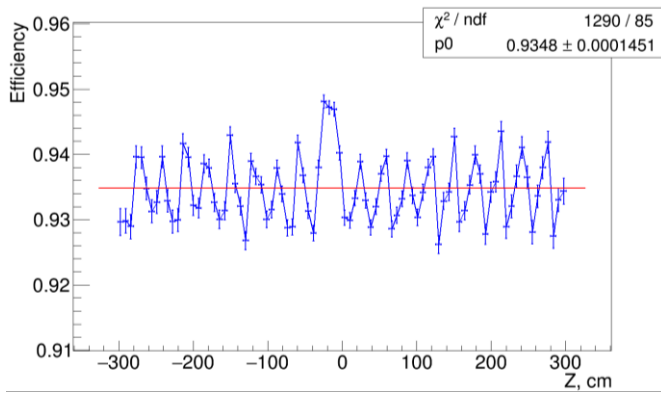


Figure 3.14: Distribution of geometric efficiency along Z direction integrated over azimuth angle.

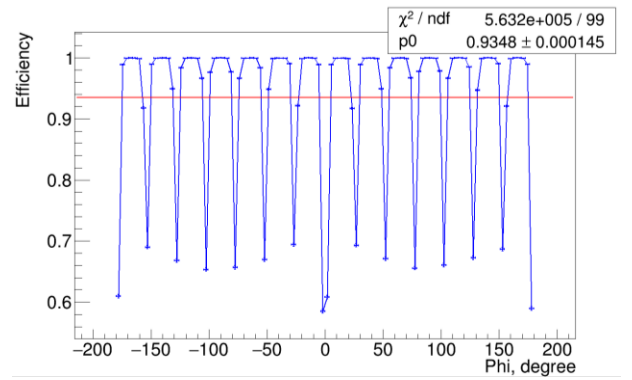


Figure 3.15: Distribution of geometric efficiency along Z direction integrated over azimuth angle.

3.4 Acceptance estimation and track matching.

P_t versus rapidity distributions of the primary hadrons reaching the TOF barrel are presented on Fig. 3.16. The events were simulated by QGSM at energy $\sqrt{s_{NN}} = 5$ GeV and 11 GeV. The produced particles were traced with the GEANT at the magnetic field $B = 0.5$ T, particle decays are also taken into account. The distributions are for the region $|\eta| < 1.4$. Different empty regions for pions, kaons and protons are due to magnetic field and polar angle acceptance. Some particles beyond the boundaries of the basic structure have a secondary origin from the decays of primary particles, and therefore fall into the acceptance of the TOF system.

Procedure of matching tracks with hits in the TOF system is to find the appropriate time for each of the reconstructed TPC tracks that have reached the TOF barrel. Number of these tracks is N_{rec_tracks} for the efficiency and contamination calculation. For a given TPC track, we have then a set of TOF strips and TOF dead regions crossed by the probe tracks. Each reconstructed TPC track has an extrapolated point with spatial window, determined by the accuracy of the Kalman track extrapolation (3σ). Hits in the TOF - candidates for matching are selected in each track window. Such candidates can be more than one in one window. The nearest to the extrapolation point candidate selected as matched with this track.

If, as a result of matching, the Kalman track and the MC hit correspond to one particle, then such track is considered to be well matched or true (N_t). If matched Kalman track does not correspond to the correct particle, then such a track is considered wrong-matched (N_w).

Therefore, the matching efficiency is calculated as: $eff = (N_t + N_w) / N_{rec_tracks}$. Contamination means the ratio of wrong-matched to the sum of wrong and true matched pairs: $cont = N_w / (N_t + N_w)$.

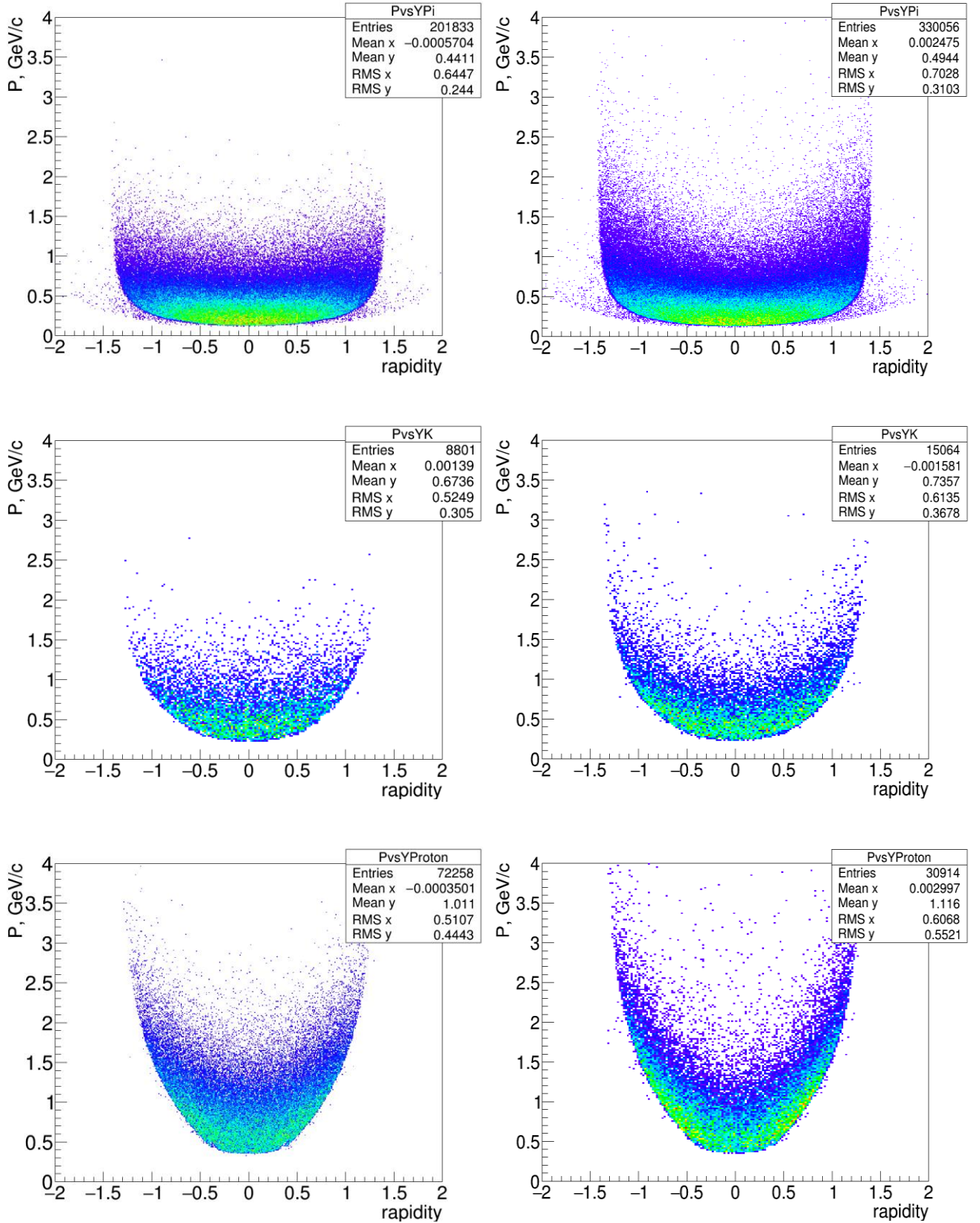


Figure 3.14: MPD TOF phase-space for charged hadrons for $\sqrt{s_{NN}} = 5$ GeV (left) and $\sqrt{s_{NN}} = 11$ GeV. From top to bottom: pions, kaons and protons. (1000 QGSM central events, $B = 0.5$ T).

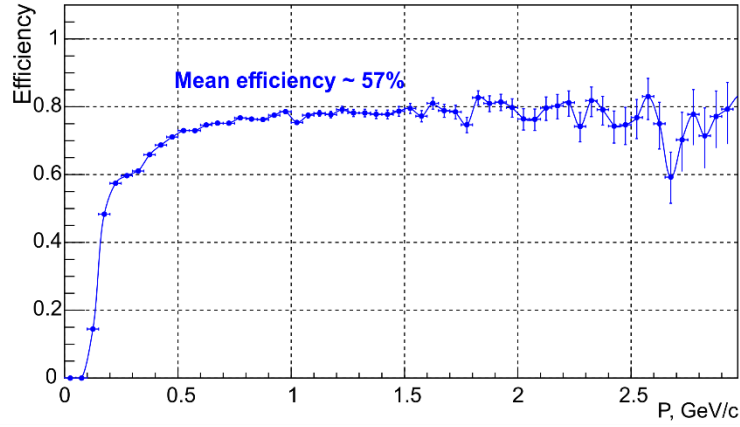


Figure 3.15: The momentum dependence of the efficiency of the TPC track matching with TOF hits for all charged particles ($\sqrt{s_{NN}} = 11$ GeV, $B = 0.5$ T).

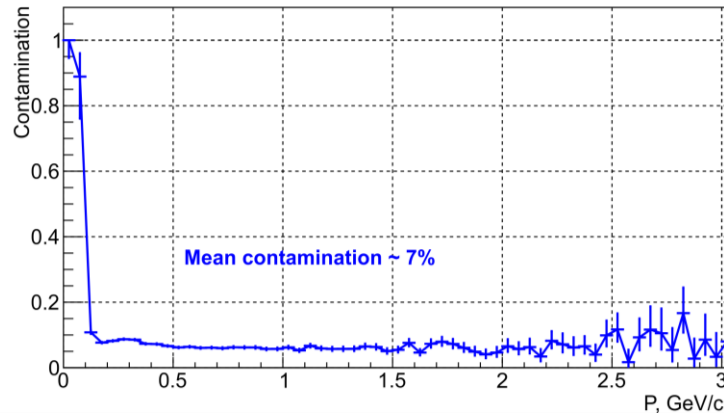


Figure 3.16. The momentum dependence of the contamination of the TPC track matching with TOF hits for all charged particles ($\sqrt{s_{NN}} = 11$ GeV, $B = 0.5$ T).

Table 3.2: Particles losses in the region $|\eta| < 1.4$ for central Au-Au collision with $\sqrt{s_{NN}} = 5$ GeV.

Mean number of primary particles in one central collision:	π^\pm		K^\pm		p	
	Produced in 4π	410.2		24.3		152.3
Produced in pseudorapidity $ \eta < 1.4$	306.4	1.0	18.4	1.0	90.0	1.0
Registered in TOF (loses due to field $B = 0.5$ T, decay and interactions, geometry efficiency)	201.8	0.66	8.8	0.48	72.3	0.80
Matched with tracks	186.2	0.61	8.4	0.46	66.3	0.74

Table 3.3: Particles losses in the region $|\eta| < 1.4$ for central Au-Au collision with $\sqrt{s_{NN}} = 11$ GeV.

Mean number of primary particles in one central collision:	π^\pm		K^\pm		P	
	Produced in 4π	829.1		58.7		153.1
Produced in pseudorapidity $ \eta < 1.4$	502.1	1.0	31.3	1.0	39.2	1.0
Registered in TOF (looses due to field $B = 0.5$ T, decay and interactions, geometry efficiency)	330.0	0.66	15.1	0.48	30.9	0.81
Matched with tracks	303.1	0.60	14.4	0.46	27.8	0.74

The momentum dependence of matching efficiency for $\sqrt{s_{NN}} = 11$ GeV is in Fig. 3.15. The contamination is presented in Fig. 3.16. In Tables 3.2 and 3.3 are summarized the absolute numbers and the fractions of different particle specie (per event) registered by the TOF detector and matched with TPC tracks.

3.5 Time-of-Flight particles identification performance

Particle's mass can be calculated using the information about the reconstructed momentum, track length and time-of-flight from the collision vertex to the TOF hit. Detector response was simulated in accordance with the processes taking place inside the TOF-module when a charged particle passing through it, the overall time resolution of the TOF system (including the resolution of the start counter) was estimated to be below 100 ps. In Fig. 3.17 an example of mass separation capabilities of the TOF MPD system is presented. The green lines show a suggested way to select particles, i.e. particles of given type which get outside of the boundary were counted as a loss of efficiency while those in other area are counted as a contamination. The MPD PID performance can be considerable enhanced using a combination of ionization loss (dE/dx) from TPC and time-of-flight measurements. An example PID plot for the momentum interval of $0.5 < p < 1.0$ GeV/c is shown in Fig. 3.18.

As the results of simulation demonstrate for a typical track length of about 1.6 m the pion/kaon separation will be achieved up to the total momentum of 1.5 GeV/c; one can select protons from other species up to $p = 3$ GeV/c.

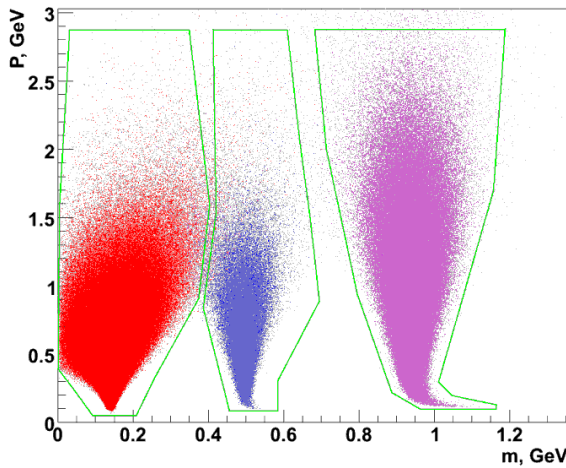


Figure 3.17: Mass separation with MPD TOF (99). The green lines show boundaries for efficiency and contamination estimation.

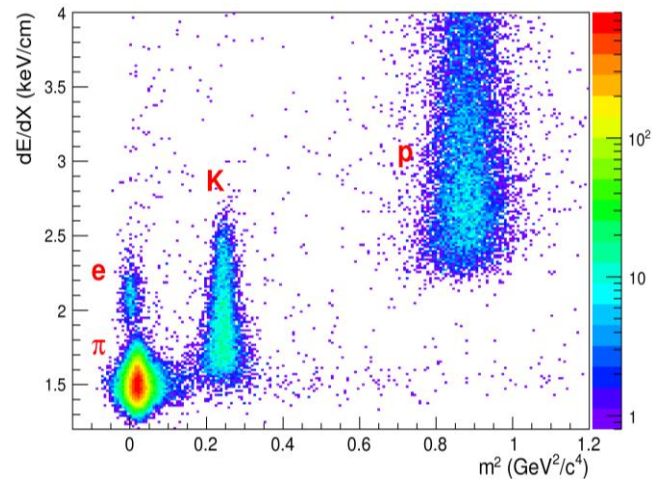


Figure 3.18: Combined dE/dx and TOF particles identification for $0.5 < p < 1$ GeV/c region.

3.6 Front-end electronics and data acquisition system

A very important part of the high performance time-of-flight system is readout electronics. For the full exploitation of the excellent timing properties of the Multigap Resistive Plate Chamber, front-end electronics with special characteristics is needed. The signals from MRPCs must be amplified and discriminated as fast as possible without lossless.

Leading and trailing times of the discriminated signal must be digitized and measured with accuracy much better than the time resolution of the detector. Readout electronics for the MPD-TOF will consist of the front-end electronics (FEE) and data acquisition system (DAQ).

3.6.1 Preamplifiers for the TOF MRPC

For the front-end electronics, we decided to use electronics like used in the TOF ALICE. Such electronics is very convenient for our TOF system. Since each detector has a 24 strip it was decided to create a 24-channel amplifier on the example of the front-end board of the TOF ALICE based on the NINO ASIC.

The NINO application-specific integrated circuit (ASIC) (Fig. 3.19) developed in 0.25 micron CMOS technology recently by the CERN LAA project, which combines a fast amplifier, discriminator and stretcher. The NINO ASIC had to satisfy the following requirements [18]: differential input; optimized to operate with 30-100 pF input capacitance; LVDS differential output; output pulse width dependent on the charge of the input signal; fast amplifier to minimize time jitter (a peaking time less than 1 ns); threshold of discriminator adjustable in the range 10 –100 fC; eight channels per ASIC. Main features of the NINO ASIC are shown in Table 3.4.

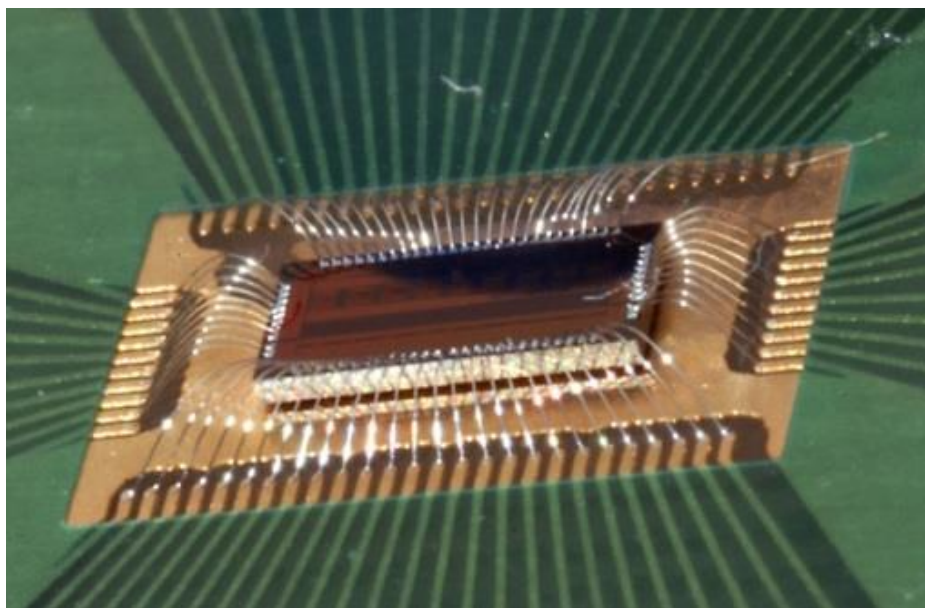


Figure. 3.19: The NINO ASIC (8 channels) directly bonded on the PC board (no packaging).

Table 3.4: NINO ASIC specifications table.

Parameter	Value
Number of channels	8
Peaking time	1 ns
Supply voltage	2.5 V
Power consumption	27 mW/ch
Input signal range	30 fC – 2 pC
Noise (with detector)	$< (2.5 - 5) \times 10^3 \text{ e}^- \text{ rms}$
Discriminator threshold	10 fC to 100 fC
Differential input impedance	$40 \Omega < Z_{in} < 75 \Omega$
Timing precision	$< 10\text{ps jitter}$
Outputs	LVDS

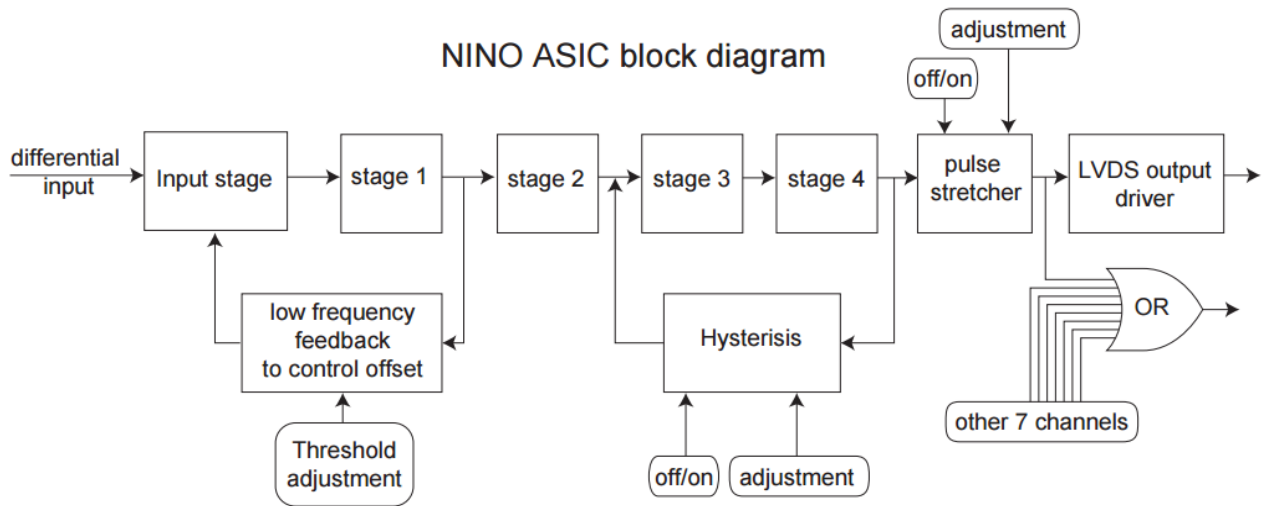


Figure 3.20: Block diagram of the NINO ASIC.

A block diagram of the NINO is shown in Fig. 3.20. The input stage is followed by 4 stages of low-gain, high-bandwidth differential amplifier ($G=6$, $BW=500\text{MHz}$). A slow feedback circuit supplies current to ensure that the input stages remain correctly biased. In addition, an offset is added at this point that acts as a threshold adjustment. There is a stretcher just before the LVDS output driver. The pulse width before stretching varies between 1 ns and 7 ns; the digitizing electronics based on the HPTDC chip [19] that will be used in the data acquisition system of the TOF MPD can only measure both leading and trailing edges of an input pulse for widths greater than 6 ns. Thus, the pulse stretcher will increase the pulse width by 10 ns.

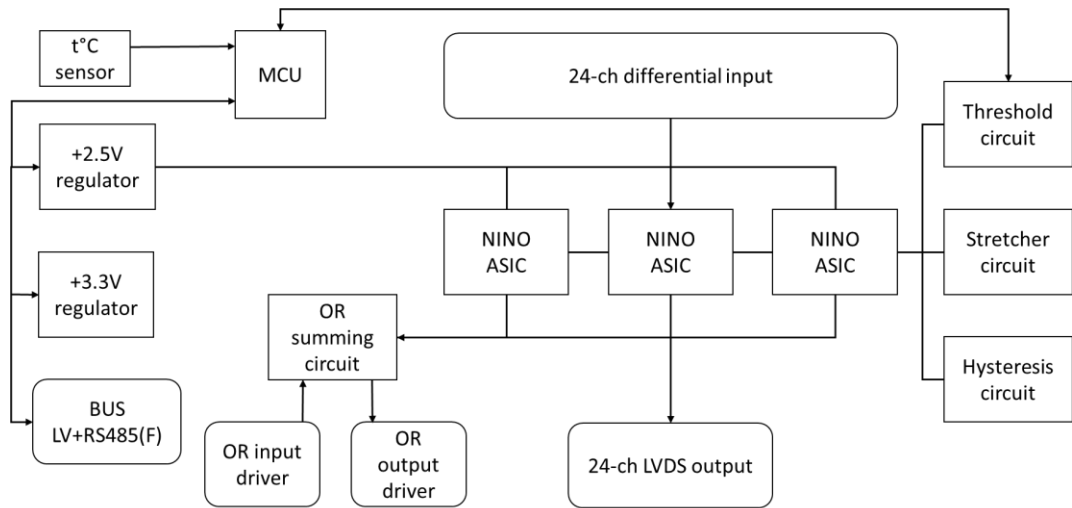


Figure 3.21: Simplified schematic of the preamplifier board for the MPD TOF system.

For the TOF MPD the 24-channel NINO based preamplifier board was developed [20]. This preamplifier board is adapted for the two-side strip readout in MRPC at the MPD experiment. Overall dimensions of the preamplifier are 196.5 x 89 mm².

Features of the MPD TOF preamplifier board:

- stabilized voltage supply of the NINO;
- the input impedance matched to impedance of the MRPC;
- overload protection at input channels;
- capacitors at the inputs for two-side strip readout;
- the possibility to use as a trigger (parallel “or” output);
- the threshold monitoring and control;
- the NINO’s voltage monitoring and control;
- the board and the gas space thermal monitoring.

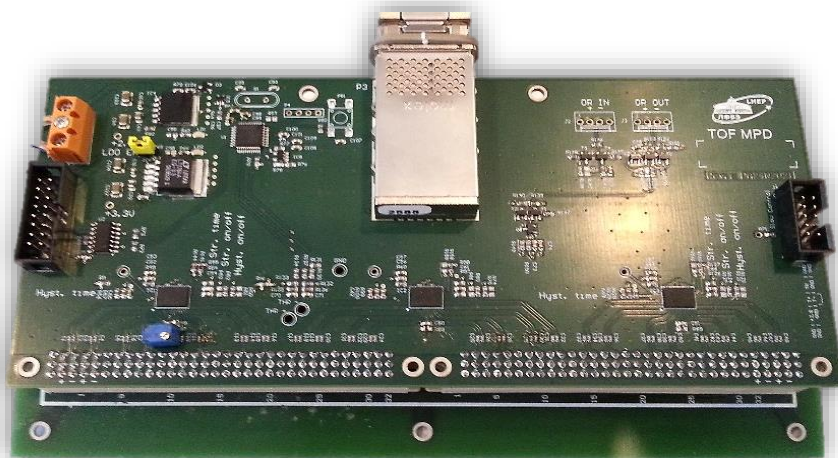


Figure 3.22: 24-channel NINO based preamplifier board with the CXP output connector.

Block-scheme of the front-end board presented in Fig. 3.21. Preamplifier board supplies by +5 V DC via connected bus, then regulating to +2.5 V DC for amplifiers and to +3.3 V DC for microcontroller. STM8L152C8T6 is used to control +2.5 V regulator, threshold and temperature acquisition from the board and the gas space. The threshold default value is 165 mV around base line 1.25 V. The stretcher and the hysteresis circuits adjusted to +1.25 V.

The preamplifier board has two DIN 41612 96abc (3 x 32) connectors as inputs and CXP connector as output (Fig. 3.22, 3.23). Each input channel terminated to the ground through 1 M Ω resistor. It allows changing the preamplifier when the high voltage applied on the detector. In addition, capacitive coupled by 1 nF capacitor. Differential pairs input impedance designed to match to the impedance of the MRPC readout strip (55 Ω) to minimize signal reflection and crosstalk.

The output preamplifier signal is in the LVDS standard. There is OR logic circuit which links all NINO and could be used as trigger.



Figure. 3.23: View of the Molex CXP Interconnect System cable.

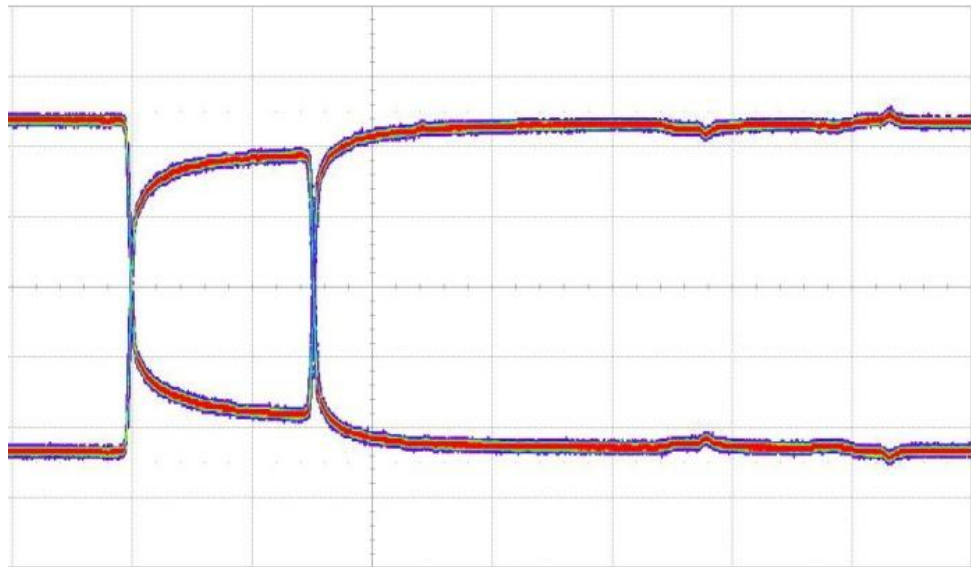


Figure 3.24: LVDS signal after passing through 5 m length Molex CXP copper cable 26 AWG, 10 ns/div.

Fig. 3.24 show the transmitting output signal from the NINO front-end board through the CXP copper cables. The CXP copper cable assembled by Molex, it has 26 AWG cable size and provides differential 100 Ω transmission line with good electrical characteristics up to 10m long.

Measured jitter between two channels of the amplifier is about 7 ps (Fig. 3.25).



Figure 3.25: The time distribution between two channels of the NINO FE board measured using the LeCroy 4 GHz oscilloscope.

3.6.2 Preamplifier's voltage supply

Stable power supply of the amplifiers and their accessories circuits is an important part, as many parameters depend on it.

We propose the following power supply circuit. +5 V DC power supply organized by MPOD low voltage source module (iSeg MPV 8016I) and 2 distribution boards (DB) connected by DC cable (stranded copper conductor with cross-section of 1.5 mm²), then to each DB connected 20 preamplifiers boards in parallel via 4 buses. Each bus controlled independently. Input voltage on preamplifier board regulated to +2.5V DC (MIC37301-2.5WR) and +3.3V DC (MIC37301-3.3WR). To compensate the voltage drop on the cables the MPOD LV source has sense pins. Total current for each channel is about 2.1 A.

This scheme tested in laboratory (Fig. 3.26). Each amplifier consumes about 0.42 Amps.

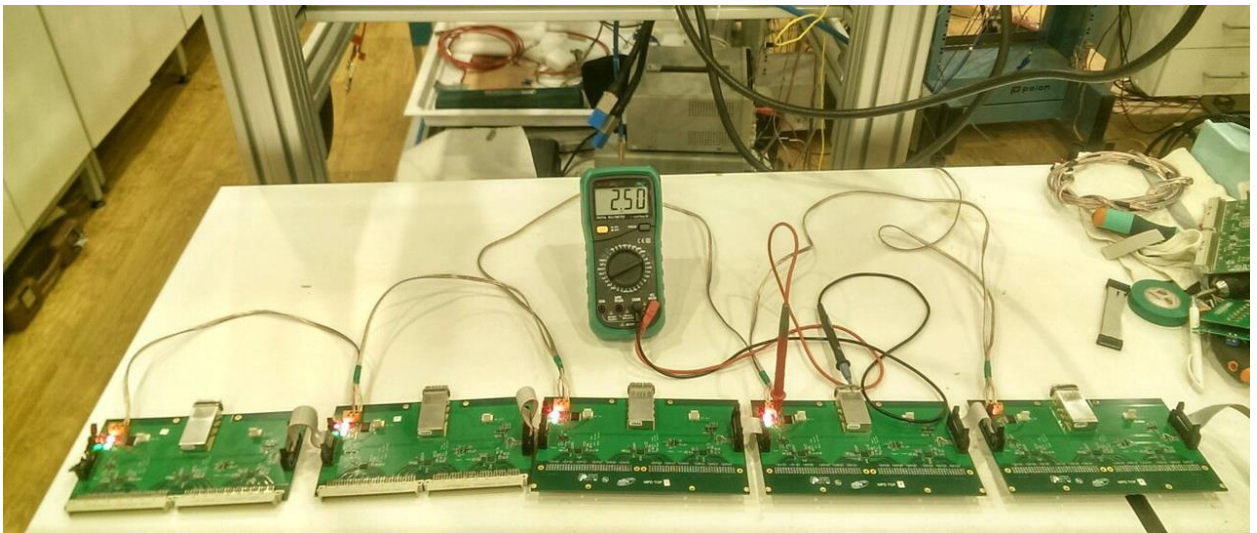


Figure 3.26: Testing of the power supply and slow control system on five preamps connected in parallel.

3.6.3 Preamplifier's control

It is necessary to control the voltage of chips and external circuits of adjustment such as stretch stage and voltage on threshold stage to achieve precise results and efficiency.

Control of the preamplifiers boards is provided by Slow-Control System which include from one side software based on TANGO toolkit and QT SDK, and other side hardware, which includes analog-digital and digital-analog converters in microcontroller (STM8L152C8T6), which installed in all FEE boards to monitor and manage voltage. Communication with the FEE boards is based on RS-485 full-duplex interface via bus and then via Ethernet by the serial port sever (MOXA NPort IA-5250). It provides access to devices from any authorized client via Internet connection.

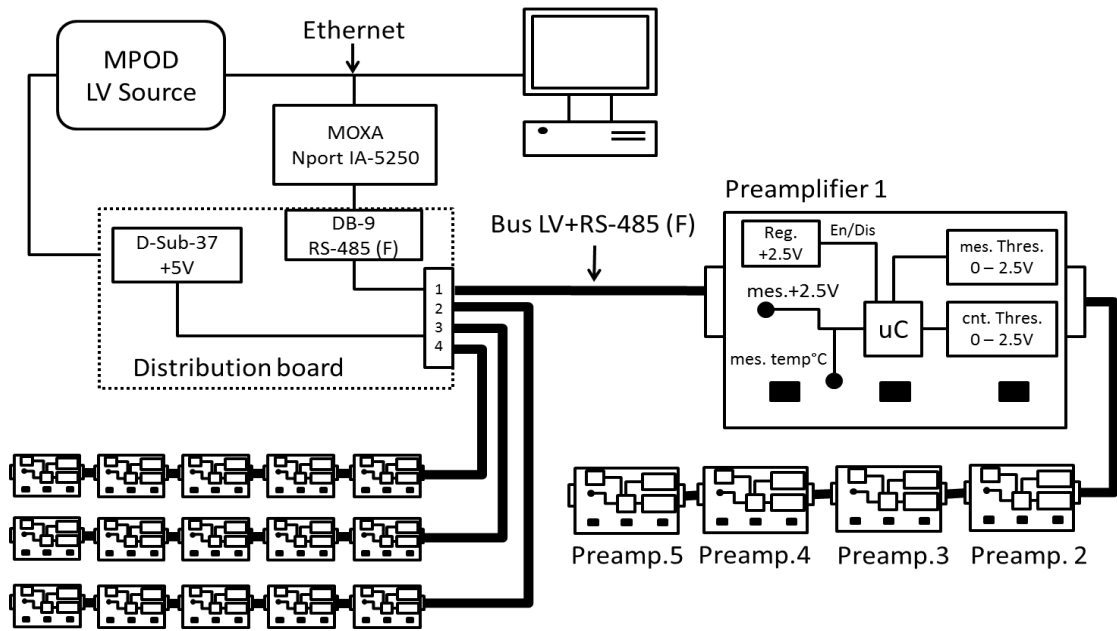


Figure 3.27: Powering Preampilfier board and connection scheme.

20 FEE boards are connected in parallel by the 20 pins twisted-pair cable to one distribution board (Fig. 3.27), where the power channels from the LV source and the signal lines are distributed to the buses. To each bus connected four FEE boards where the MAX3070E transceiver installed. These transceivers communicate with serial port server (MOXA NPort IA-5250) via RS-485 interface then serial port server via the Ethernet with PC. Monitoring and control interface are available via the Internet simply using a special developed client's application with graphical user interface (Fig. 3.28).

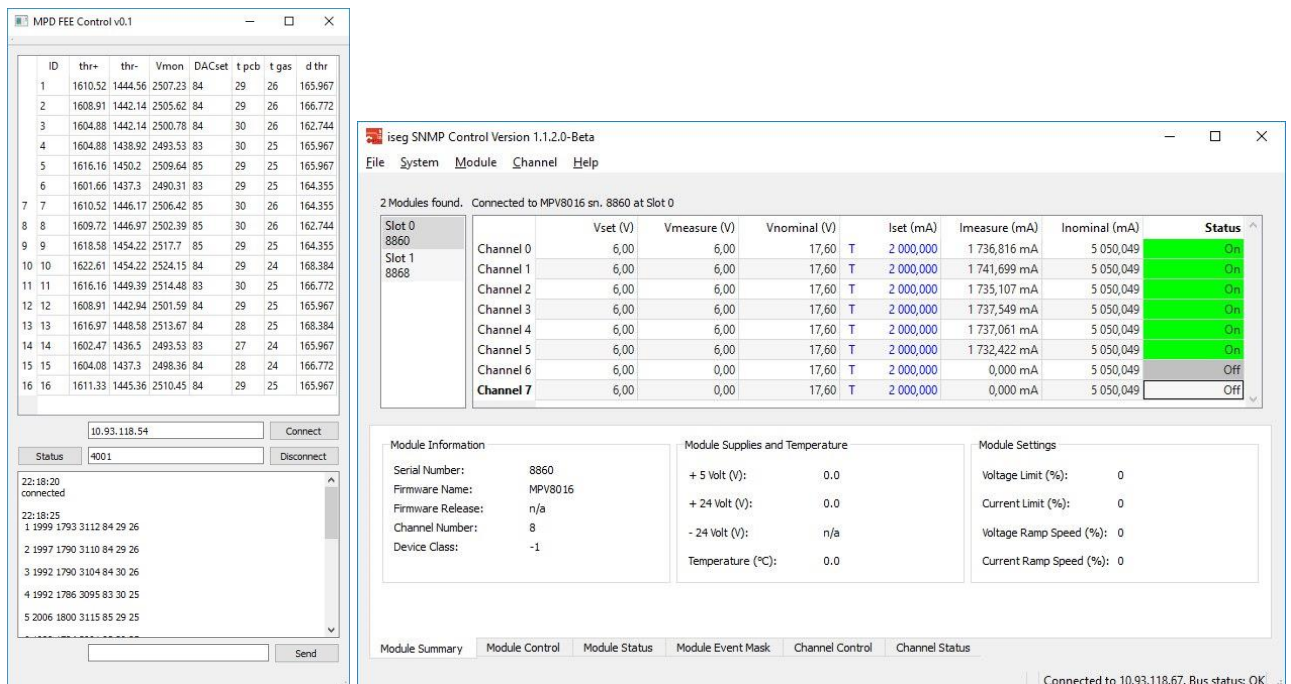


Figure 3.28: Slow control GUI clients(left side for FEE, right LV source).

3.6.4 Time-Over-Threshold method

The signal amplitude must be taken into account in time measurements. The time-amplitude correction can significantly improve the time resolution. The NINO pulse width is somewhat dependent on the MRPC pulse height. Thus, the integral of the pulse (charge) can be obtained by measuring the pulse width. Time correction using the LVDS pulse width is called the “Time-Over-Threshold” (ToT) method. Because this method requires only time information, it can simplify and reduce the cost of readout electronics.

The dependence of the width of the LVDS pulse on the charge at the input of the NINO preamplifier is shown in Fig. 3.29. A wide range of width for small amplitudes allows making corrections more accurate in the areas with the highest jitter of the input signal. An example of the “time-over-threshold” distribution for the strip readout MRPC is shown in Fig. 3.30. This distribution should be reduced to a linear form (to 0) to improve the time resolution. That correction improves the time resolution of the detector is almost twice (Fig. 3.31, 3.32).

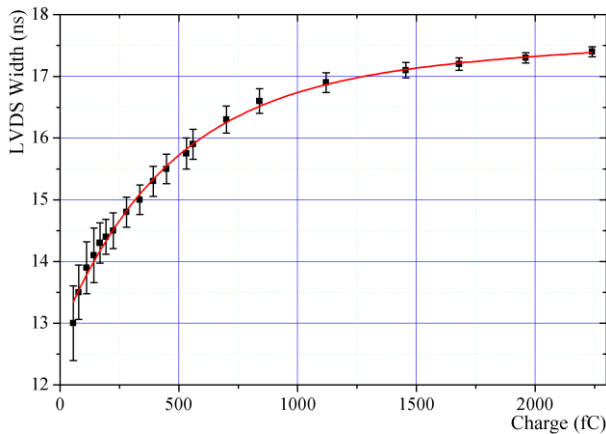


Figure 3.29: Charge dependence of the width of the output LVDS impulse from NINO preamplifier.

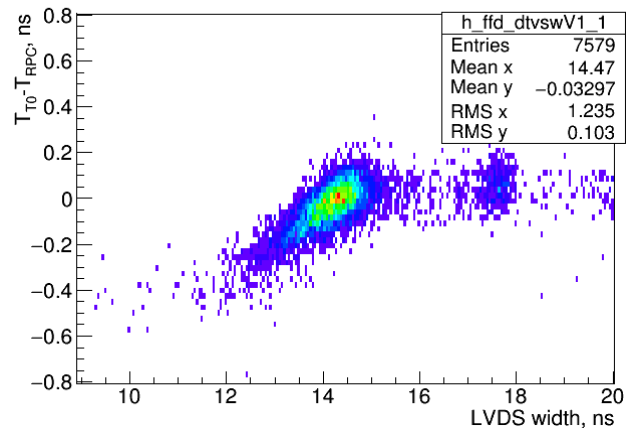


Figure 3.30: Example of the “time-over-threshold” curve with the time-width distribution.

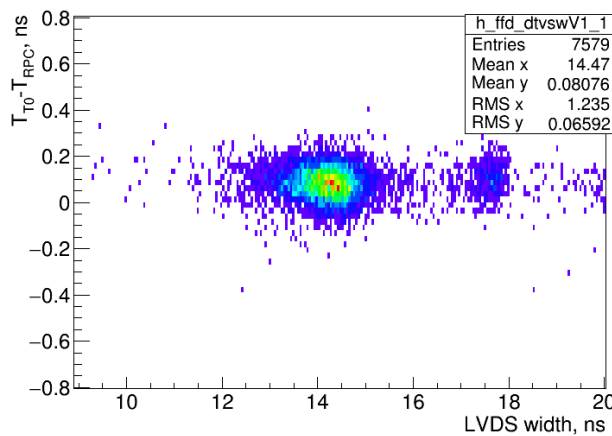


Figure 3.31: Corrected width-time distribution.

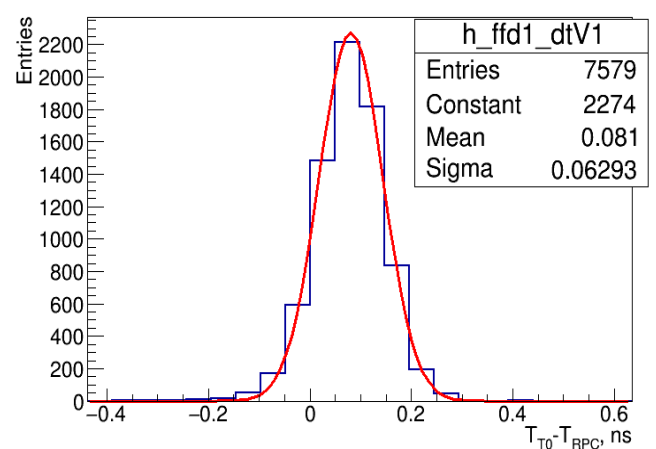


Figure 3.32: TOF distribution after correction.

3.6.5 Time-to-digital converter TDC72VHL



Figure 3.33: Time-to-digital converter TDC72VHL with the CXP input connector.

Figure 3.34: Electronics for the data acquisition system in the VME rack.

New VME64x time-to-digital converter TDC72VHL (Fig. 3.33) based on HPTDC chip was designed for MPD TOF readout. It is used for digitizing LVDS signals coming from the output of the NINO amplifier. One VME module has 72 differential inputs ($100\ \Omega$) and produced with the same type of connectors as on the preamplifier. Three amplifiers can be connected to one such module. Time sampling of the TDC72VHL is 24.4 ps per bin. The TDC72VHL provides the ability of the precise “White Rabbit” [21] synchronization with other timing devices and can operate in standalone mode. One VME rack can hold up to 18 of the TDC72VHL (Fig. 3.34). The total amount of the TDC for the TOF MPD is 196 (14 modules per each of 14 VME crates).

The main estimated parameters of the TOF DAQ are in Table 3.5. The data rate calculated from average occupancy $\sim 15\%$ and means trigger rate ~ 6000 Hz. Average number of fired channels in one interaction is $6720 \times 0.15 \approx 1000$. Event size in this case calculated as $1000 \times 2 \times 12 = 24$ kBytes. Data rate is $24\text{kB} \times 6000\ \text{Hz} \approx 144\ \text{MB/s} \approx 1.2\ \text{Gb/s}$.

Table 3.5: TOF DAQ estimation parameters.

Parameter	Value
Raw data information type	Lead+trail time, 24.4 ps/bin
Channel size	12 Bytes
Average event size	24 kBytes
Maximum data rate	$< 1.2\ \text{Gb/s}$
Maximum number of TDC72VHL	196
Total power	3500 W

3.7 Weight and material budget of the TOF system

Details of the evaluation of the module weight are given in Table 3.6. Weight of the one TOF module not more than only 130 kg. It means that the device for installation and servicing of the TOF modules could be simple and light. The total mass of the full TOF barrel (14 sectors) is thus about 3700 kg.

Table 3.6: Weights of the TOF module components.

Part	Weight, kg
1 MRPC	6.5
2 covers and support plate per module	45
FEE, cables, connectors per module	30
Total per module	140
Total per barrel	3640

The calculated contributions of all parts of the TOF to the radiation length of one average Module are listed in Table 3.7. In overlap region (less than 10% of all effective surfaces) of the MRPC radiation length reaches 21.5%. This amount of material will affect the quality of the ECal insignificantly. Work to optimize the design of the detector is underway in order to reduce its radiation length.

Table 3.7: The MPD TOF material budget.

Material	Radiation Length X/X_0 (%)	Total contribution of
18 MRPC glass plates	4.3	MRPC: 7.5%
2 plates of Honeycomb	0.2	
4 PC boards	3	
Gas box cover	1.1	box: 4.5%
Central support plate	2,3	
Top cover	1.1	
FEE & IC	1	electronics: 2%
Cables	1	
Total	14	

3.8 Area for mass-production of the TOF MRPC

Since 2014 area (Fig 3.35) for the mass production of detectors is created in the laboratory. The workshop consists of the several areas (Figs. 3.36 – 3.41):

- ultrasonic cleaning glass;
- drying the glass;
- painting conductive HV layer;
- assembly and check of the MRPC;
- assembly of the modules;
- test of the assembled modules on cosmic.

The technology of the assembling of detectors was developed at the beginning of 2015 when 6 MRPCs was assembled in the area for mass-production for the BM@N experiment and studying at the "Test MPD" setup. The cleaning of the glass is carried out in two stages. First, the glasses are cleaned in the ultrasonic bath with a special surfactant, and washed with deionized water, which is purified by reverse osmosis filter in a special cleaning system. After washing, the glass is dried in special drying oven, and then it comes to the area for assembly detectors. MRPC assembly takes place on the tables made of massive granite slabs to avoid detector deformation during gluing and assembly. The detailed description of the assembly procedure is given below.

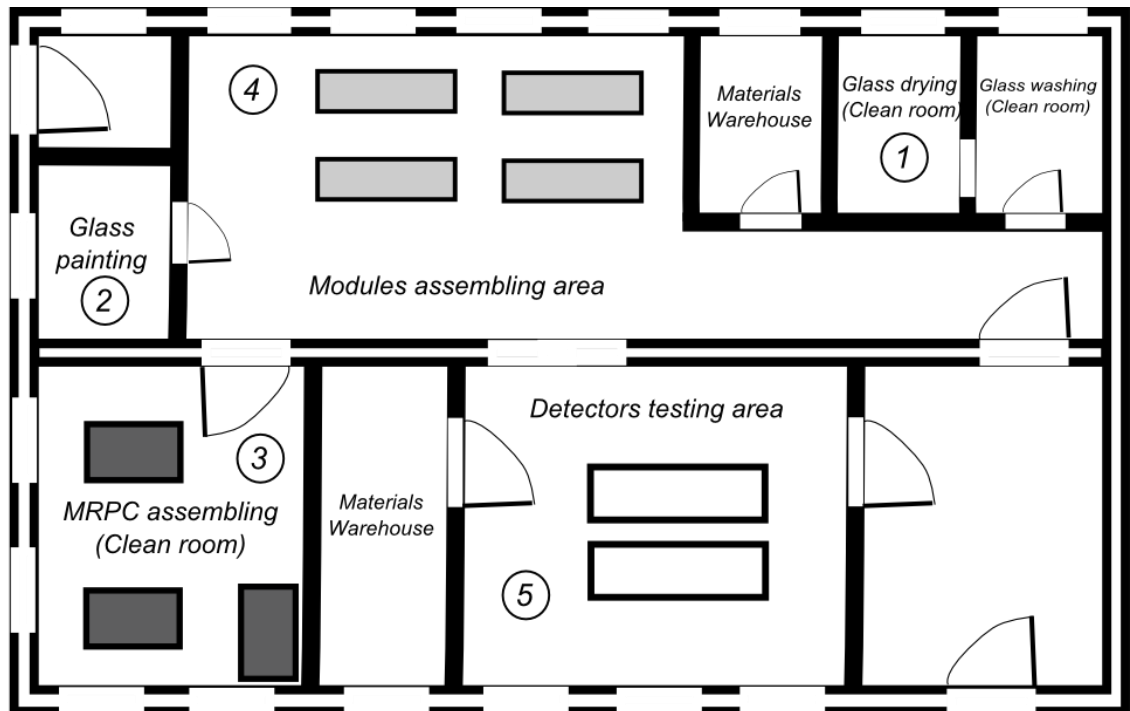


Figure 3.35: Scheme of the MRPC mass production workshop.



Figure 3.36: Ultrasonic cleaning of glass.

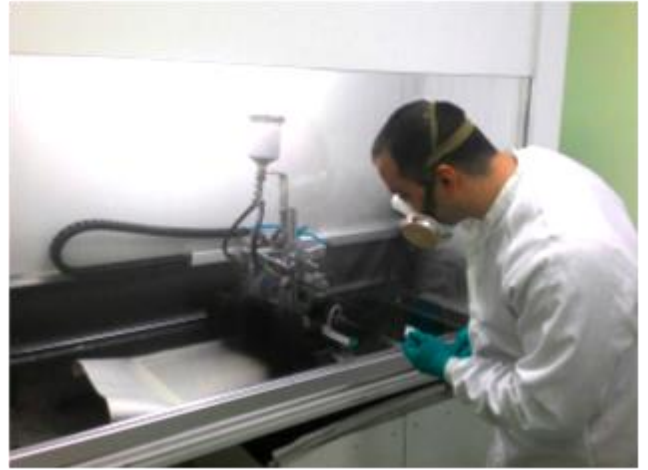


Figure 3.37: Painting of the conductive HV layer.



Figure 3.38: MRPCs assembling in the clean room.



Figure 3.39: Check of the MRPC assembling quality.



Figure 3.40: Soldering of the signal cables.

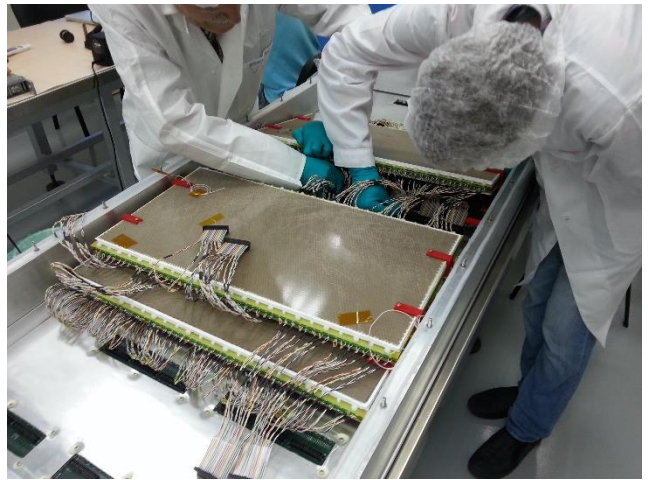


Figure 3.41: TOF module assembling procedure.

3.9 Step-by-step MRPC assembling procedure

Materials for the assembly of the MRPC are commercially available. The list of materials to produce one detector is shown in Table 3.8. The assembly procedure is presented graphically in Fig. 3.42.

Table 3.8: Components and materials for the production of one MRPC detector.

Name of material or component	Dimensions	Quantity
Aramide honeycomb panel with 0.5 mm	640x300x5 mm ³	2 pcs
Fiberglass PCB with strips (inner)	645x330x2 mm ³	2 pcs
Fiberglass PCB without strips (outer)	645x330x2 mm ³	2 pcs
Float glass (inner)	640x300x0.27 mm ³	12 pcs
(outer)	640x300x0.4 mm ³	6 pcs
Monofilament fishing line	∅ 0.2 mm	100 meters
PET screws with nuts	M5 x 20 mm	40 pcs
Mylar sheets	640x300x0.1 mm ³	6 pcs
Kapton adhesive tape	10 mm width	10 m
Copper adhesive tape	10 mm width	10 cm
Double-sided adhesive tape	20-30 mm width	10 cm
Special conductive paint	-	100 ml
Twisted pair cable 3M (16 pairs)	0.25 m	6 pcs
Teflon coated wire	0.35 mm ²	2 m

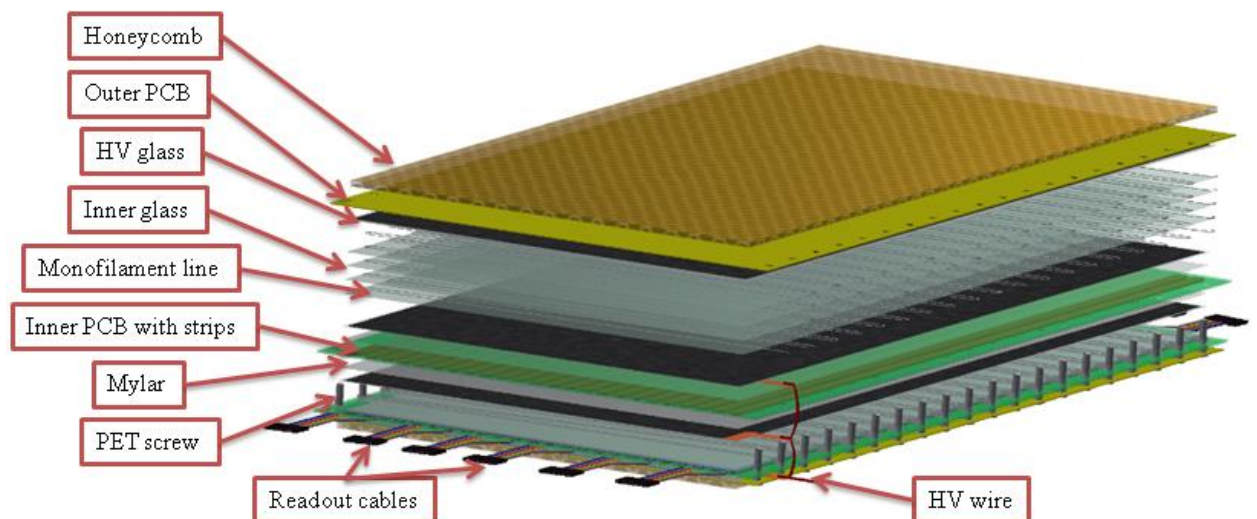


Figure. 3.42: The sequence of operations of the MRPC assembly.

There are four main areas (rooms) in the workshop (see Fig. 3.35):

1. Clean rooms for washing and drying glass.
2. Room for applying the conductive paint to the glass.
3. Clean room for the MRPC detectors assembling.
4. Hall for modules assembling and testing.

Procedures to do in the area 1 (washing and drying):

1. The required number of glasses is checked for defects (splits, cracks and dirty) and measured their thickness.
2. Glasses rinsed ordinary water to wash away particles of glass dust.
3. Container with glasses is placed into the ultrasonic bath with special detergent where the glasses are washed for 10 minutes at the temperature of about 50 °C.
4. Glass after cleaning in the ultrasonic bath thoroughly washed under a shower of deionized water to wash away the detergent residues.
5. Container with washed glasses is placed in a drying oven for 1 hour at the temperature of 70 °C.
6. Glasses in container after drying are moved from the oven to the closed shelves in the same room.
7. Container with clean glasses is transferred to the assembly room.

Procedures to do in the area 2 (painting conductive layer):

1. Container with cleaned outer glasses brought to the room for applying conductive layer.
2. Preparation of glass for coating by conductive layer:
 - 2.1. Each glass is taken out from the container and is blown by “ionizer” for preventing the adhesion of dust.
 - 2.2. Glasses are placed on the painting surface so that the paint consumption was minimal.
 - 2.3. The high-voltage contact is glued on the glass to the side for painting.
 - 2.4. Glass fixed on the edges by adhesive tape (3-5 mm from the edge of the glass).
3. Prepared glasses are placed in a fume hood.
4. The first layer of paint applied on the glass and dried by blow-dryer for 5 minutes.
5. The second layer is applied and also dried for 5 minutes.
6. The glasses are placed in a drying oven for 12 hours at a temperature of 90 °C.
7. Painted and dried glasses removed from the oven.
8. The adhesive tape removed carefully (so as not to damage the edge of the paint and glass).
9. Surface resistance is measured at the 6 – 10 points of the conductive layer. It must be within 5 – 20 MΩ/□.
10. Ready-to-assemble glasses transferred to the assembling room.

Procedures to do in the area 3 (MRPC assembling):

1. Honeycomb panels are glued to the PCB:
 - 1.1. In the special place outside the clean room the surface of the honeycomb panel treated sandpaper and wiped with isopropyl alcohol.
 - 1.2. Clean PCB's are transferred on the granite table for gluing with honeycomb panels.
 - 1.3. The surface of the PCB with strips wiped with isopropyl alcohol.
 - 1.4. Epoxy adhesive applied on the surface of the honeycomb panel.
 - 1.5. Honeycomb panel is pressed to the outer side of the PCB without strips and pressed down by the load (for example lead bricks).
 - 1.6. The adhesive dries completely within 24 hours.
 - 1.7. Surface is checked for flatness by mechanical method.
 - 1.8. Boards with glued panels are ready for assembly.
2. Preparation of the external PCB for assembling:
 - 2.1. The external PCB with honeycomb panel placed on the granite table.
 - 2.2. The external glass sheet is put to the PCB, the surface painted with the resistive paint facing the PCB.
 - 2.3. Wire soldered to high voltage contact and insulated by polyimide tape.
 - 2.4. Glass is glued on the edges to the PCB by the 10 mm polyimide (Kapton) adhesive tape.
 - 2.5. Plastic screws are installed to holes at the long edge of the PCB.
 - 2.6. Board is immovably fixed to the table.
3. Monofilament diameter of 0.2 mm binds to the first screw.
4. Monofilament is wound on the screws in the form of a triangle.
5. Mylar strips (5 mm width) are glued to the both short edges of the inner thin glass.
6. Inner thin glass (with) placed on the monofilament fishing line.
7. Steps 4 – 6 are repeated until the five layers of monofilament fishing line will lie in the stack.
8. Preparation of the internal readout electrode:
 - 8.1. Next glass with conductive coating puts conductive paint down on the one PCB of the internal electrode. The high-voltage contact must be positioned on the PCB so that the anode and cathode contacts located on the diagonal.
 - 8.2. Wire soldered to inner high voltage contact and insulated by polyimide tape.
 - 8.3. Glass glued around the perimeter of a polyimide tape 10 mm (3-5 mm from the edge).
 - 8.4. The internal electrode is laid glass side down to the 5th layer of the monofilament line of the first glass stack. Before lying, the both surfaces are blown by ionizer.
 - 8.5. The PCB is pressed tightly to the line.

9. Third glass with conductive coating puts conductive paint down on the other side of the internal electrode in accordance with items 8.2 – 8.4. High voltage contact must be at the same position that on the other side of the internal electrode.
10. Second stack assembled as the first one in order of 3 – 7.
11. Second internal readout electrode assembled as the first one in order of 8 – 9.
12. Third stack assembled as the first and the second in order of 3 – 7.
13. The upper outer board prepared in accordance with step 2 and placed on the last fishing line layer in the third stack.
14. The Assembled detector is carefully pressed down by lead brick and stacks fixed by PET nut.
15. The twisted pair cable soldered to each strip (two pairs for one strip).
16. The IDC-32 connector is set on the free end of the cable.
17. The ready detector checked for defects on the special stand.
 - 17.1. Cracks searched by laser.
 - 17.2. Glass plates' integrity in the assembled MRPC is controlled with video camera.
 - 17.3. The readout differential line checked for the absence of reflections and the quality of the electrical contacts with generator and oscilloscope.

Procedures to do in the area 4 (the TOF module assembling):

1. The module box is placed on the table.
2. The first detector is fixed to the box in the recess.
3. The remained detectors are stacked and fixed in a box.
4. After the installation of the detectors the lid is fixed above the box.
5. Connect all the connectors inside.
6. Close lid and fix it by screws.
7. Test module on gas tightness.

3.10 TOF modules installation

The MPD TOF is lightweight construction. Calculation of the mass of the TOF module has shown that the maximum mass is 150 kg with all accessories. From this, we can conclude that for installation and service of the TOF system does not need a complicated and heavy device. As well, structures for fixation of the module inside the barrel could be lightweight and simple. In 933 this case, the following variant is proposed.

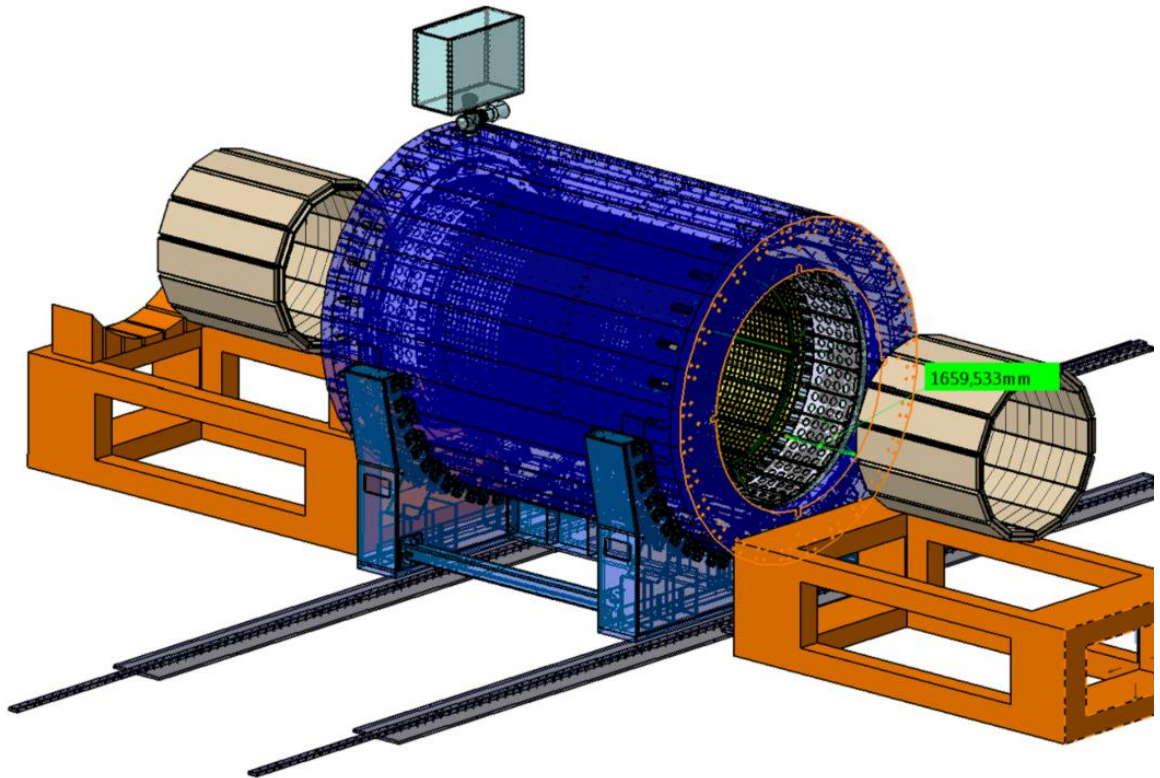


Figure. 3.43: The TOF installation into the MPD barrel.

The installation of the TOF will begin after the finishing of the ECal installation. Each module will be inserted in their position on both sides of the yoke of magnet (Fig. 3.43). This will be done by means of a mobile support structure. The structure is equipped with adjustable rails of the same kind used inside the MPD barrel. To insert a module into the barrel it is enough to suspend the support structure with the hall crane in front of the chosen services sector and connect the rails together to form a unique sliding line that will allow pushing the module into the right position. The supporting structure will be designed in such a way as to allow the positioning of the module at the different angles corresponding to the ones of the sectors. The requested positioning precision is not high (of the order of a millimeter), so a simple mechanical reference is sufficient to define the position.

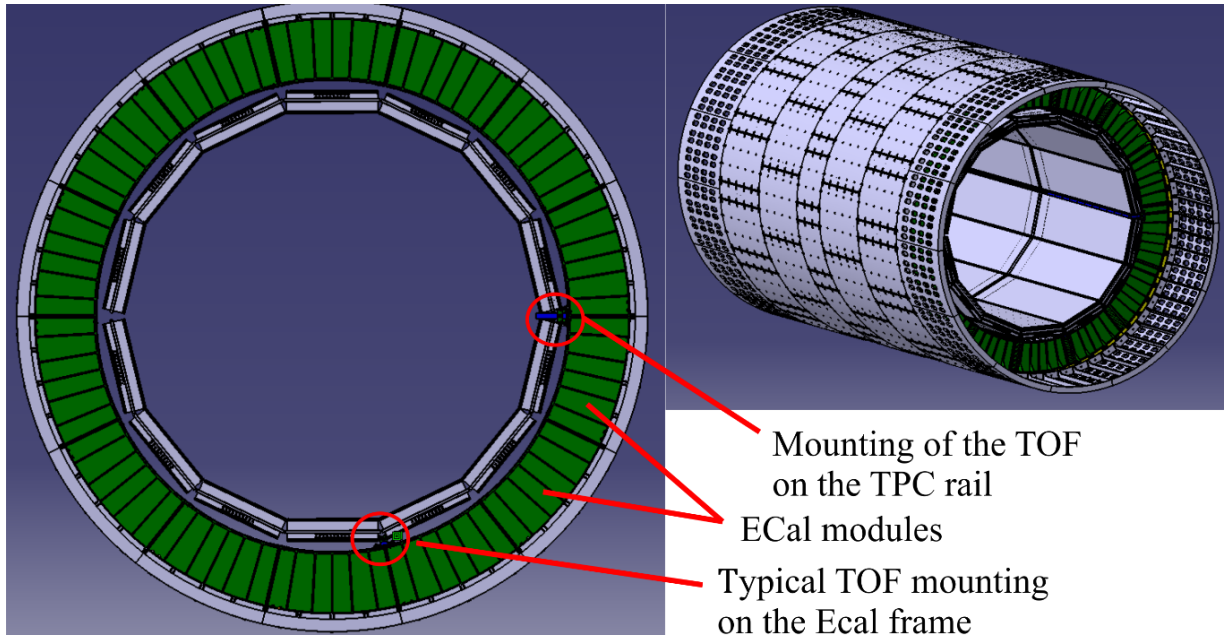


Figure. 3.44: Two types of the TOF mounting rails on the ECal frame.

For convenient installation of modules inside the barrel, they are equipped with roller guides (Fig. 3.45). All detectors inside the barrel will be mounted to the ECal frame using two types of special rails with slots (Fig. 3.46). In typical case, the TOF module is set in the corresponding slots on the rails by means of snap all the way into the stop flange. Then a conical pin centers it. The final fixing is performed by pressing the flange, which is positioned on the rail by means of pins. Such a system facilitates installation and service of the modules.

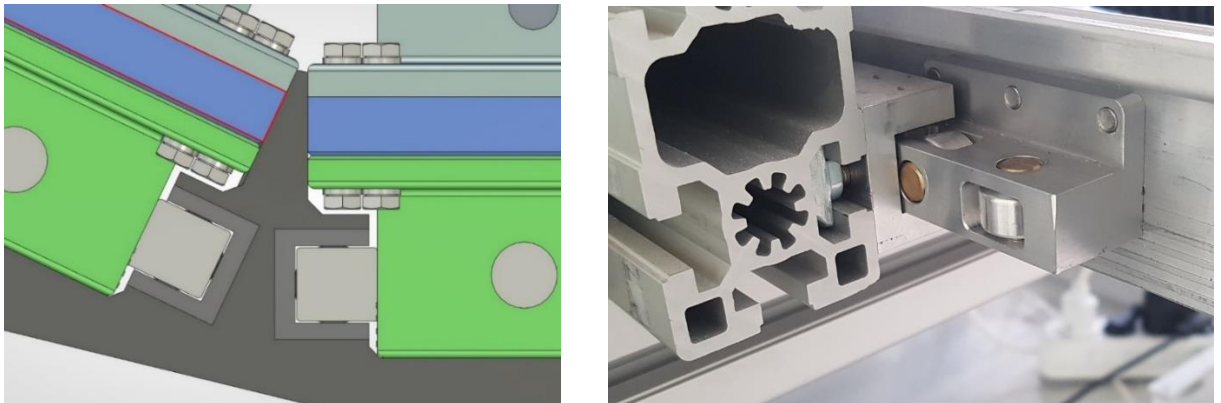


Figure. 3.45: Roller guides on the TOF module.

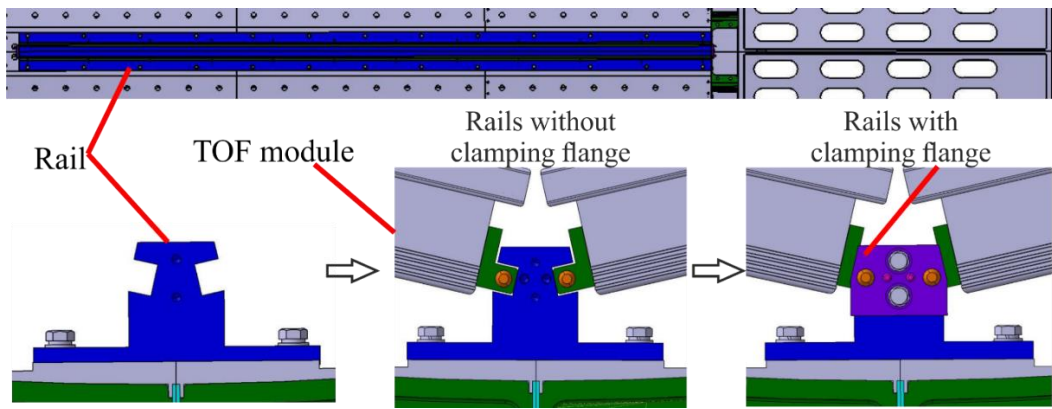


Figure. 3.46: Standard fixation procedure of the TOF module on the ECal frame.

In the case of fastening with the horizontal rail of the TPC, mounting of modules made similarly with a typical case. The change affects only construction of the rail (Fig. 3.47). It is composed of three parts that are tightened by bolts. Just like in the typical installation of modules, the final fixing of the module is performed by pressing the flange to the pins.

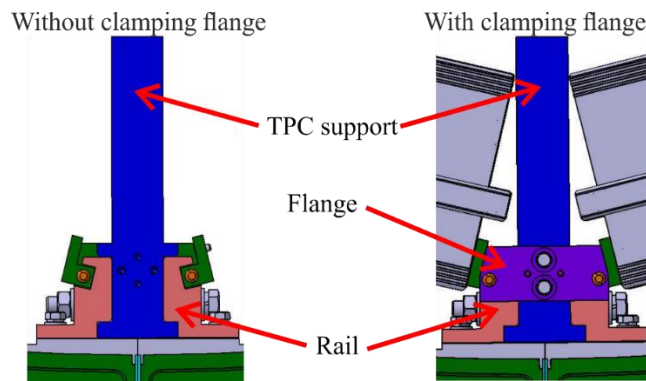


Figure. 3.47: Fixation of the TOF module on the TPC support rail.

A special device (slipway) for assembling the module, its transportation and installation inside the superconducting solenoid of the MPD is being developed (Fig. 3.48). The device should provide reliable fixation of the module during the entire time of assembly, transportation and allow easy installation the module in the MPD using a crane or a lift.

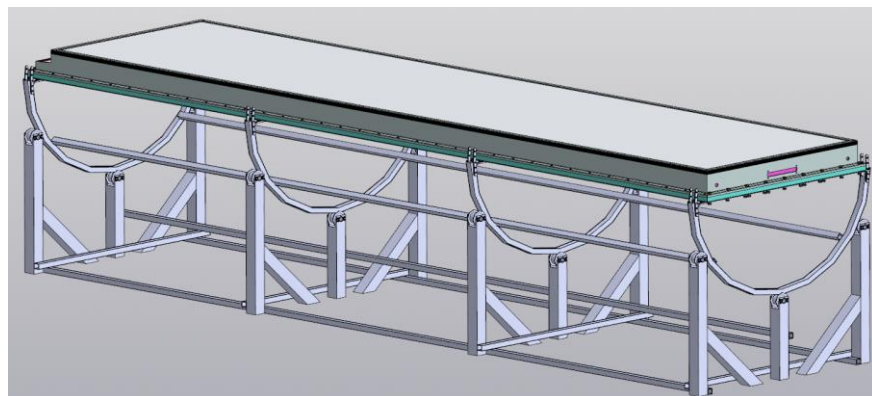


Figure. 3.48: Assembly and transport device design.

4 Service

4.1 Gas system

The TOF detectors will be operated with a non-flammable Freon rich gas mixture containing 90% C₂H₂F₄ + 5% i-C₄H₁₀ + 5% SF₆. The total gas volume of the barrel is approximately 3000 liters taking into account the volume occupied by detectors. Volumes of all elements of the TOF system are presented in the Table 4.1.

Table 4.1: Volumes of the elements of the MPD TOF.

	Number of detectors	Gas volume without MRPC detectors, liters	Gas volume with detectors, liters
Detector	1		5
Module	10	155	105
Sector	20	310	210
TOF Barrel	280	4340, ~4.3 m ³	2940, ~3 m ³

4.1.1 Simple gas system for testing elements of the TOF

Now we use simple gas systems without reflow for MRPC tests. Gas systems are almost identical both at the cosmic stand and at the MPD Test setup (see chapter 2.3). This system is based on the MKS 1479A controller. The flows of component gases will be metered by the MKS mass flow meters, which have an absolute precision of 0.3% under constant conditions. Flows will be monitored by a process control computer, which continuously calculates and adjusts the mixture percentages supplied to the system. The flow of the gas mixture can be adjusted in range from 3 l/hour up to 20 l/hour but running flows will be typically about 30% of full-scale flow on the mass flow controllers. Gas will successively blow modules and go out to atmosphere through the oil bubbler.

Table 4.2: Parameters of the existed “Test beam MPD” gas system.

Parameter	Value
Gases	C ₂ H ₂ F ₄ , i-C ₄ H ₁₀ , SF ₆
Number of channels	4
Maximum flow rate	20 l/hour
Reflow system	No
Working pressure	< 2 bar

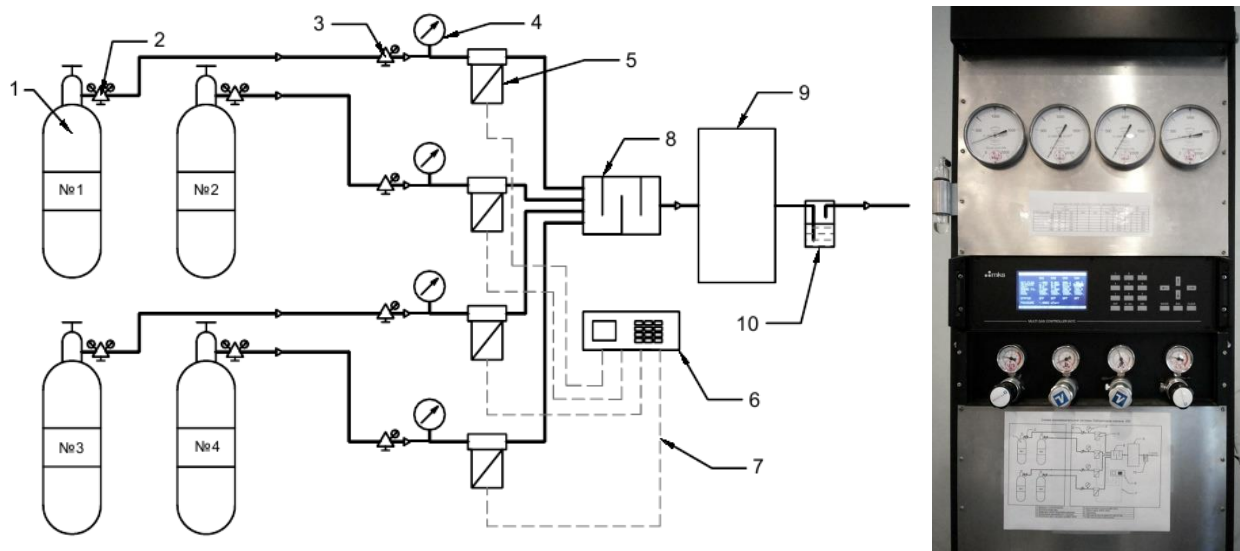


Figure 4.1: The scheme of the MRPC gas system at the MPD Test area: 1 – gas bottles; 2 – gas pressure regulator; 3 – safety gas pressure regulator; 4 – control manometer; 5 – MKS1479A flow meter; 6 – MKS647C gas controller; 7 – interface cables; 8 – gas mixer; 9 – detector; 10 – oil flap.

4.1.2 Proposed closed loop circulation gas system

Principal scheme of the closed loop gas distribution system is shown in Fig. 4.2. Proposed system will provide mixture 90% C₂H₂F₄/5% i-C₄H₁₀/5% SF₆ to the ToF chambers with proper pressure and purity. Because of bad influence on environment and high cost of the gases, system will work in closed loop circulation mode. Slow Control system will remotely control process, while Data Acquisition system will collect system and gas mixture parameters.

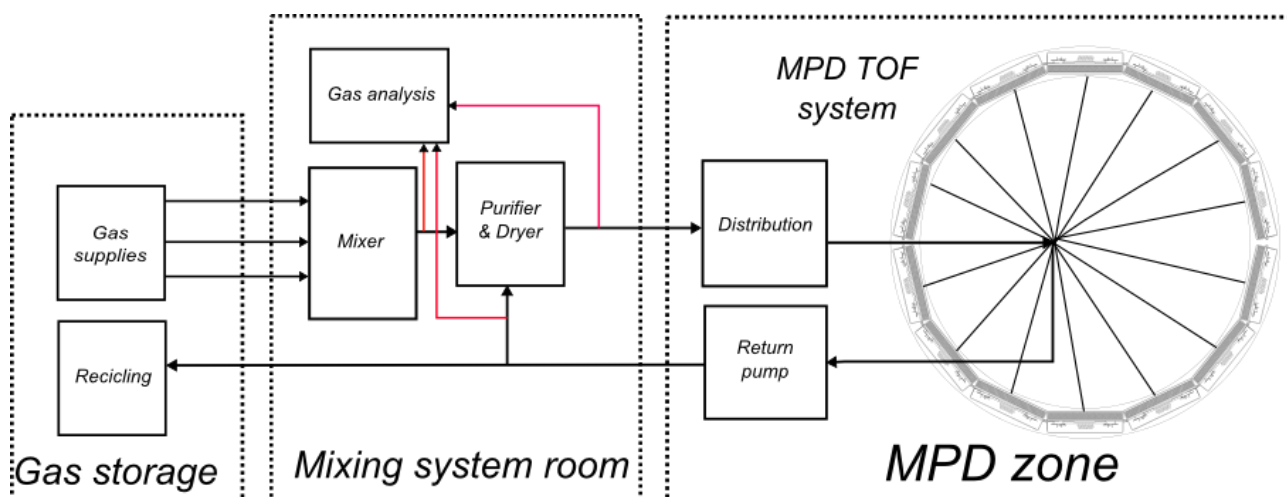


Figure 4.2: Schematic view of the proposed TOF closed loop gas distribution system.

4.1.2.1 Gas supply & Mixer

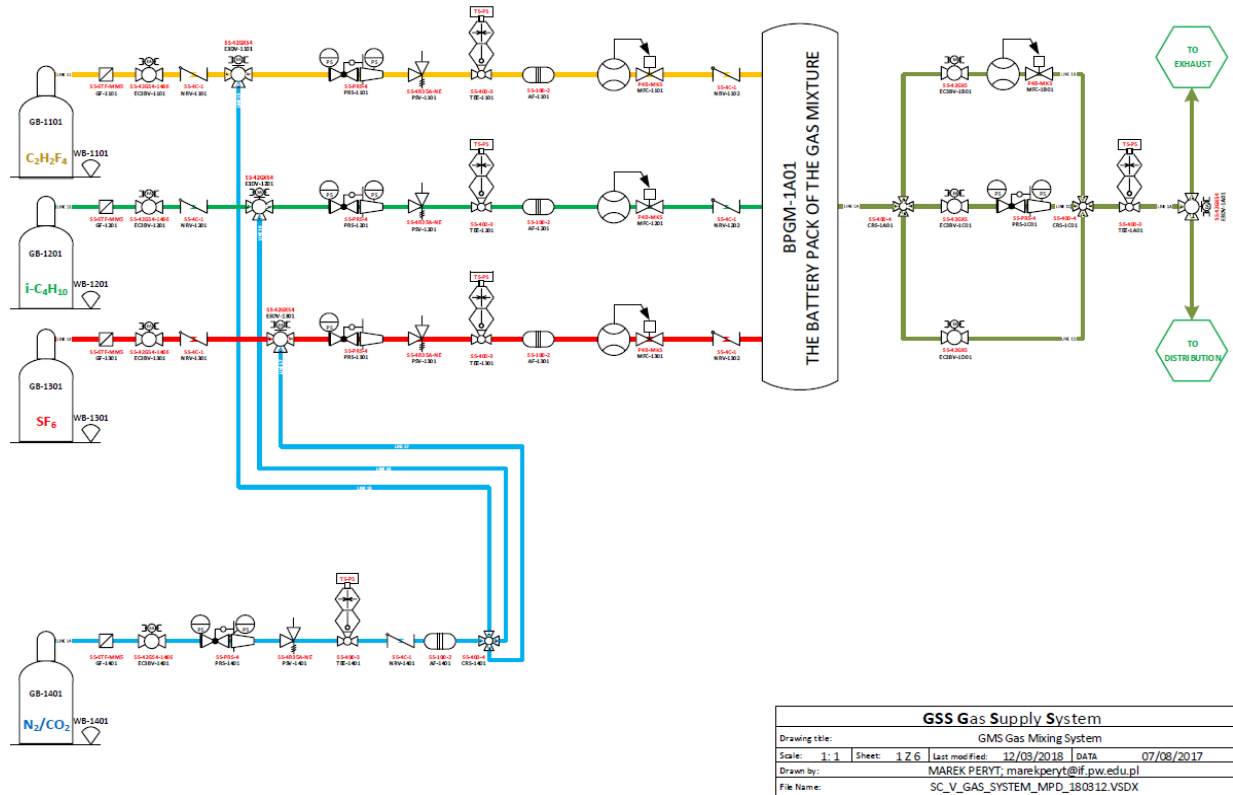


Figure 4.3: Scheme of the gas mixer.

Gas supply is a place from where fresh gases will be taken. Amount of the gases in the cylinders will be measured by industrial weighting modules connected with Slow Control system. Gas Mixer (Fig. 4.3) will ensure correct ratio of the gases. Main parts of this module will be mass flow controllers – master controller for $C_2H_2F_4$ with controllers $i-C_4H_{10}$ and SF_6 slaved. It may be necessary to use two mass flow controllers for every gas, one for filling operation and another for running. The difference between flows during these operations is relatively high, what may have bad influence on precision of the measurements while using one device for both purposes. This part of the system will also consist pipeline with mass flow controller for pre-purging detector with high flow of $C_2H_2F_4$.

4.1.2.2 Analyzer

Quality of gas mixture properties are essential for proper work of the system. Isobutane is flammable gas and its content has to stay under specified limits. High amount of water and oxygen may disrupt results of the experiment. Gas analyzer will monitor their content in the mixture. This information will be used to calculate necessary flow of the mixture in the purifier module. During normal operation portion of gas mixture will be taken from the circulation. Analyzer module will provide ability to measure gas mixture separately from various parts of whole Gas System.

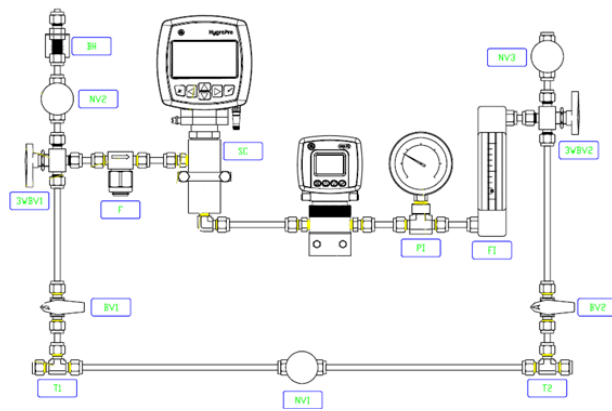


Figure 4.4: Scheme and photo of the gas analyzing system.

4.1.2.3 Purifier

To provide low water and oxygen content purifier module will be used. It will consist two parallel columns filled with copper catalyst (to remove oxygen) and molecular sieve (to remove moisture). During normal operation we expect to use one of them. Second will be reserve, used if regeneration during operation will be necessary or another incident happen. Purification module (Fig. 4.5) will also consist pipelines, valves heater and other required equipment used for columns regeneration.

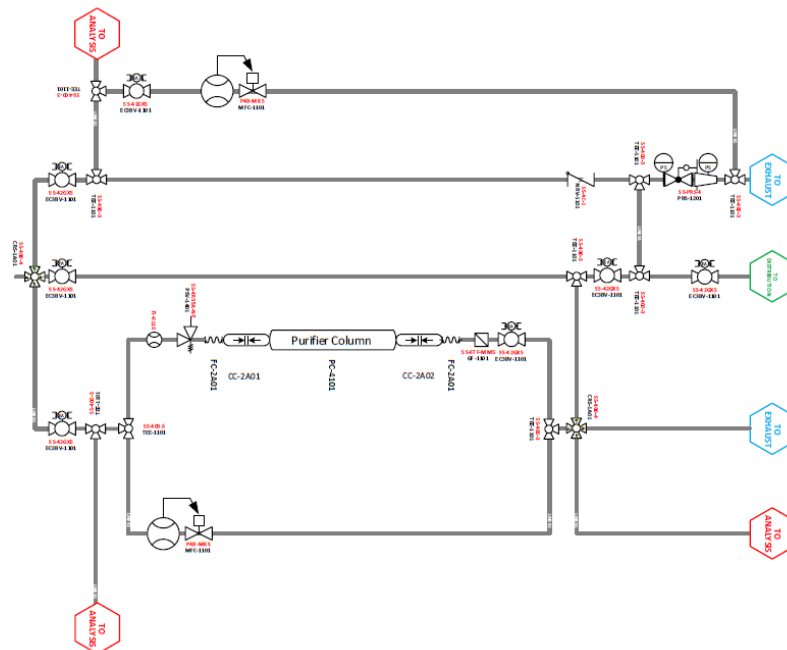


Figure 4.5: Scheme of the purifier.

4.1.2.4 Distribution

The barrel of the Time-of-Flight system of the MPD consists of 14 sectors. Each sector contains 2 gas boxes. Each box must be supplied gas independently (Fig. 4.6) to be able to dismantle

any module without disconnecting the other. Distribution system will divide stream and deliver necessary amount of gas in every ToF segment. It will also contain pressure and temperature indicators to monitor gas parameters. Pipe diameters vary to ensure that each module will have the same gas flow.

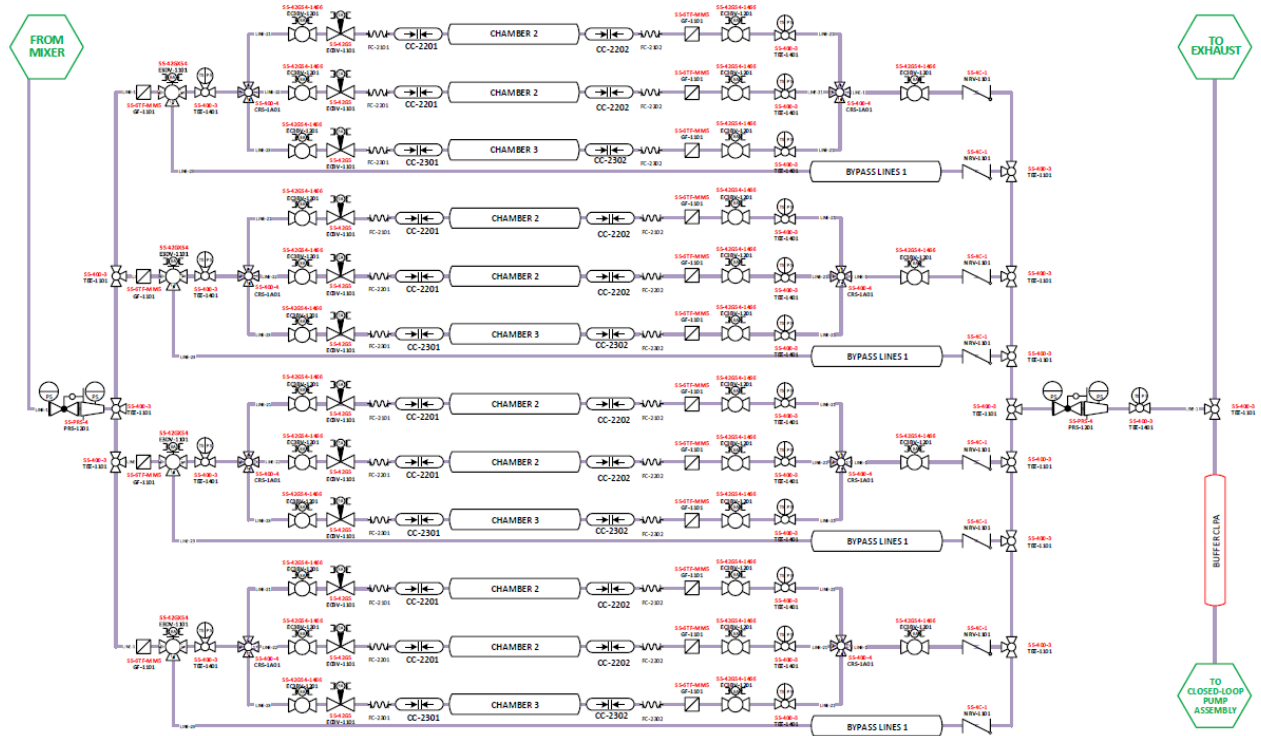


Figure. 4.6: The MPD TOF gas distribution scheme.

4.1.2.5 Compressor

Main task of compressor module will be to pump gas returning from ToF chambers to recirculation. It will contain two compressors (one reserve) and electromagnetic valves regulated by PID controller. Some part of gas mixture from the outlet of the compressor will be returned to its inlet. This solution, connected with pressure transmitter will provide ability to control pressure inside ToF chambers.

4.1.2.6 Recycling and pressure control

During operation some amount of used mixture will be compressed to the gas cylinders and its place will take fresh mixture. Pressure inside whole system will be monitored and controlled by pressure transmitters, control valves, back pressure control valves and compressor module. Pressure inside ToF chambers will be maintained at level 3-5mbar over current atmospheric pressure. Output pressure from the compressor will not exceed few hundreds millibars overpressure.

4.2 High Voltage supplies

The detector element of the TOF system, the MRPC, will be operated with a differential voltage of about ± 6 kV, i.e. ~ 12 kV across each of the three 5 gap stacks. The maximum expected rate at the MPD experiment will be of the order of 20 Hz/cm^2 (see Ch. 1.3.3). Assuming that the average charge produced by minimum ionizing particle is average 3 pC [22] for 10 gaps of $250 \mu\text{m}$, we can expect mean charge for our triple-stack MRPC is about 4 pC. The current and the power consumption of the TOF detector can be evaluated as shown in Table 4.7. The measured power consumption and the values quoted in Table 4.3 confirm that the MRPCs are low power devices.

Table 4.3: Estimates of the current and power for the HV system.

	Current	Power
MRPC	144 nA	1.73 mW
Module (10 MRPCs)	1.44 μA	17.3 mW
Sector (2 modules)	2.88 μA	34.6 mW
Whole TOF system (14 sectors)	$\sim 40 \mu\text{A}$	$\sim 0.48 \text{ W}$

A multi-channel high voltage system with remote control and a relatively small cost needed. In the case of supplying of half TOF module (5 detectors) from one differential channel (± 6 kV) of a power supply we need only 56 HV differential channels. Such number of HV channels is small and we can use simple modular HV system. The iSeg EHS 4080p(n) module, providing up to 8 kV and 1 mA, in groups of 4 channels, is currently under consideration. In this case, there will be enough 14 modules with positive polarity and 14 modules with negative polarity to supply the entire system. The power supply modules will be housed in two Mpod (Fig. 4.8) crates [23]; this will allow accurate remote control and monitoring of single channel parameters (trip, limits, current, etc.).

We will use two crates for the positive and other two for the negative voltage channels. Each detector inside the module will be connected to one of four connectors of positive or negative polarity (Fig. 4.5). Standard LEMO RG-58 50Ω HV cables with Radiall SHV connectors can be used to connect each supply channel to a module (length of around 20 meters).

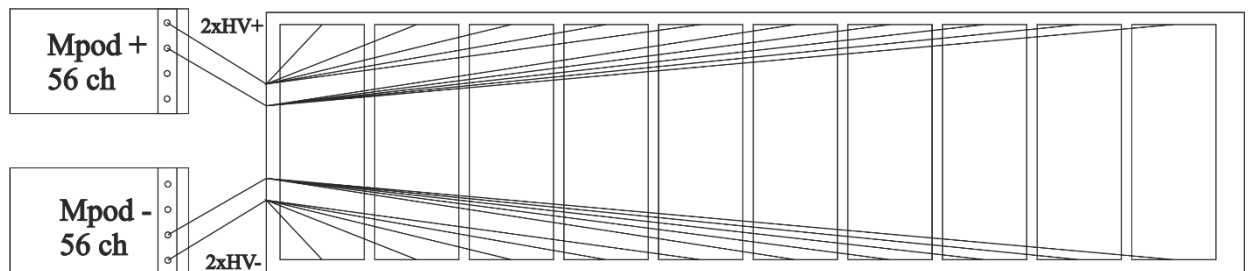


Figure. 4.7: The HV distribution scheme for one TOF module.

4.3 Low Voltage power distribution



Figure. 4.8: "W-IE-NE-R" MPod crate and 8-channel LV power supply MPV 8016I.

The power consumption of one FE card is 1.5 W. The total power consumption of the TOF is less than 850 W. Such a small power allows using a simple and cheap power supply scheme. We stopped on a variant where power supplies are located outside the MPD magnet in the experimental hall, delivering the needed voltage and current directly to the load.

The closest location for the power supplies is at ~ 12 m on each side of the barrel. The TOF system is subdivided in 14+14 half sectors (modules). Each half sector needs ~ 30 W at 3.5 V for the analogue electronics. Two "W-IE-NE-R" MPod crates (Fig. 4.8) with 8 LV supply modules (MPV 8016I) are enough to power all preamps of the TOF system. Mpod low voltage modules have 8 channels with a maximum of 50W per channel in different voltage ranges. All channels are individually controlled and monitored and have floating, individually sensed outputs.

Schematic diagram of the MPD TOF low voltage distribution is shown in the figure 4.9. One Mpod crate used to supply voltage to 7 modules. The voltage supplies to one module through 4 cables (one cable for five FE cards) of 12 m length. Each cable line will draw a current of about 2.1 A (see chapter 3.6.2). Allowing maximum 3.5 V voltage drop through the 12 m line, the cross section of each LV cable is of order 1.5 mm^2 . So needs to set voltage not more than 7 V on the power supply to provide voltage 3.5 V for each preamplifier. This connection scheme is the most optimal now.

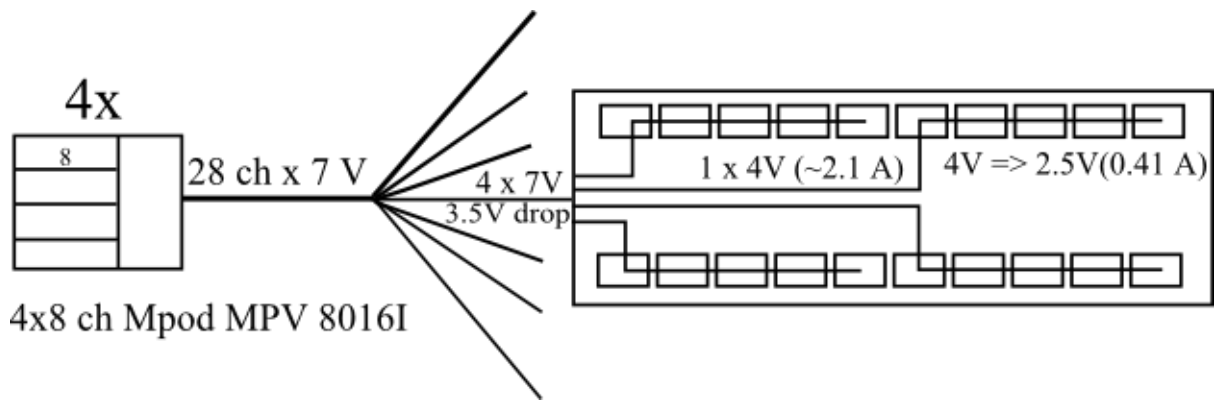


Figure. 4.9: Schematic diagram of the TOF low voltage distribution.

4.4 Slow control for the TOF system

Slow control system (SCS) refers to a computer system that monitors and/or controls multiple systems for failure prevention, monitoring and provides direct control by user or automated control.

User interaction with SCS for MPD is based on a toolkit named TANGO Control System [24], which also is being used at the Nuclotron in JINR. TANGO is a software for building control systems, which unify access to hardware. Hardware can range from single bits of digital input/output up to sophisticated detector systems.

All connections with devices are based on Ethernet. For devices without network access, like temperature sensors with RS-485 interface, Serial-to-Ethernet MOXA NPort convertors are applied. Acquired data from devices is being archived into database for further analysis and handling. TANGO control system provides handy tools for browsing data history.

The Time-of-Flight system of the MPD is necessary to monitor several parameters of different subsystems such as temperature monitoring, voltage monitoring, gas flow monitoring, etc. subsystems with controlled parameters and control devices are listed in Table 4.5. At present, most of the slow control system has been developed and continues to develop. In the right column of the table indicated the planned additions and changes of the system.

An example of the voltage and temperature monitoring which was carried during test run on the BM@N is shown in Fig. 4.10.

Table 4.5: Status of the TOF slow-control system.

TOF Subsystem	Monitored value	Devices for monitoring, realized	Planned
Detector	Temperature, pressure	Up to 255 on single line DS1624-based temperature sensors.	Honeywell HSCDRRN005PD2A5 pressure sensors.
Gas system	Flow, pressure	4-channel MKS 647C and MKS 247C gas flow controllers.	Readout and control directly from the MKS 1479A.
Low Voltage	Voltage, current	10-channel ICP DAS PET-7017-10 voltage monitoring.	Integrated voltage and current control.
High Voltage	Voltage, current	CAEN N471A source current monitoring by 10-channel ICP DAS PET-7017-10.	Integrated voltage and current control and monitoring.
Front-End Electronics	Voltage, threshold	ICP DAS PET-7017-10 voltage monitoring.	Threshold control and monitoring.
DAQ, Readout Electronics	Temperature, voltage, current	---	Read values to the database.

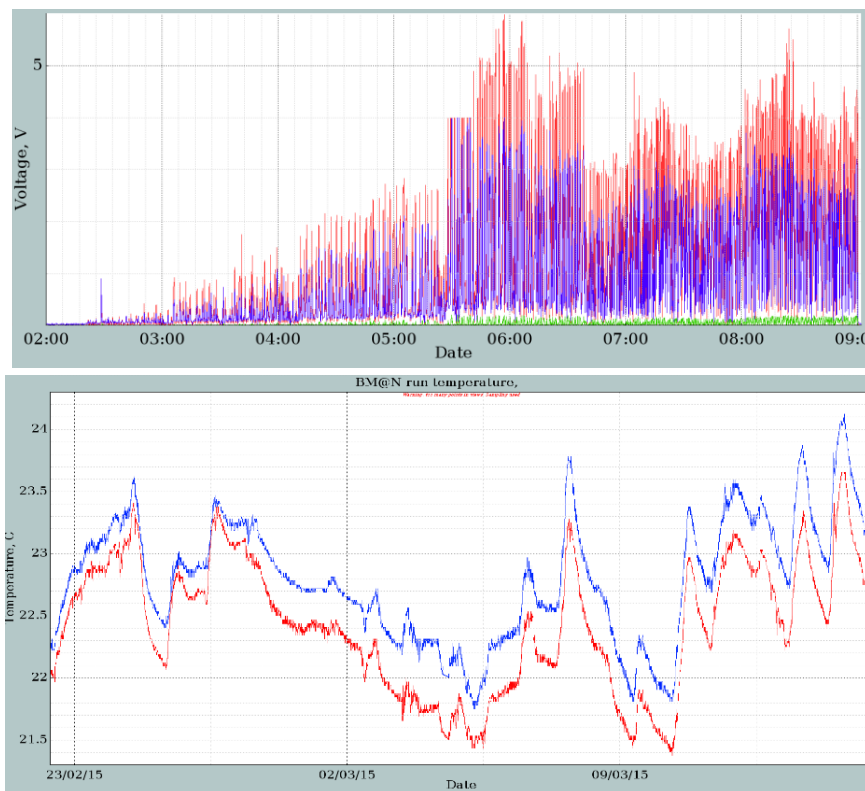


Figure 4.10: TANGO example of the voltage and temperature monitoring.

4.5 Power consumption and cooling

All power consumption can be divided into two parts: consumption of devices placed inside the magnet (unwanted heat) and outside of the magnet yoke.

There is only one volume inside the TOF barrel which maximum power dissipation of about 1 kW. As already shown in chapter 3.3.2, the power consumption of each amplifier is ~1 W. Also power cables and voltage regulators also emit some heat. Maximum 20 W/m² of the thermal power is dissipated to the space over the gas box by the Front-End Electronics with LV cables.

The readout electronics (VME crates with TDCs) will be located outside the magnet yoke and will not affect to the inner volume of the MPD. Power consumption of the one VME crate with 14 TDCs is 300 W (4200 W total for readout electronics). A rack with service equipment (LV, HV, slow control) which power consumption about 3 kW will be located in the experimental hall. Finally, the electronics of the gas system can consume about 1 kW of power.

Total power consumption foreseen for the TOF subsystems is 8 kW (see Table 4.6).

Table 4.6: TOF subsystems power consumption.

Part	Power, W
Power of FEEs with LV modules, crates, cables	1400
Power of Readout Electronics (TDC)	4200
Power of HV modules	600
Power of slow control devices	800
Power of the gas system	1000
Total	8000

Proper cooling of front-end and readout electronics is needed to prevent damages/fire and to satisfy the temperature requirements of the MPD central region (detector surface below 25°C).

Most optimal way of cooling for such heat dissipation is the use of system based only on radiators and using closed loop of air. In this case the active substance causes the temperature changes is only air. However, this method does not let to control temperature with good accuracy. Low cost and less possibility of corruption support this one option. It is going to prepare computers models that will show the efficiency of the air-cooling. After this simulation, the decision to use air-cooling will be taken.

5 Organization and cost estimation

5.1 Organization

The Time-of-Flight is subsystem of the MPD experiment and organized according MPD collaboration rules. Five organizations are committed to the development and construction of the TOF system. They are listed at page 1. Responsible persons for each subsystem and item are listed in Table 5.1. The TOF system construction leader is V.A. Babkin (JINR).

Table 5.1. Responsibilities in the TOF system project.

Working group	Chair (deputy)
Detectors & testing prototypes	V.A. Babkin (M.M. Romyantcev)
Modules	V.A. Petrov (A.V. Litomin)
Front-end electronics	M.G. Buryakov (S.V. Volgin)
Read-out architecture	S.N. Bazylev (I.V. Slepnev)
Gas system	M.J. Peryt (D. Dąbrowski)
Slow control	V.B. Shutov (D.V. Egorov)
Mechanics	S.I. Kakurin (P.O. Dulov)

5.2 Cost and resources

The cost of the TOF system split into mechanics, detectors, electronics, modules, read-out, slow control and other services is shown in Table 5.2. The manpower includes physicists, technicians and engineers who directly participate in the design, assembly and commissioning of subsystems.

Table 5.2. Manpower and cost estimation table for the TOF system construction.

Item	Manpower	Material and production cost (k\$)
Detectors & testing prototypes	5	1100
Modules	6	570
Front-end electronics	3	730
Read-out	7	1000
Gas system	5	200
Slow control	3	50
Mechanics	7	350
Total	36	4000

References

- [1] The MultiPurpose Detector (MPD), Conceptual Design Report, v1.4, http://nica.jinr.ru/files/CDR_MPD/MPD_CDR_en.pdf.
- [2] Kh.U. Abraamyan *et al.*, Nucl. Instr. Meth. **A628** (2011) 99.
- [3] K. Adcox *et al.* (PHENIX Collaboration), Phys. Rev. **C69**, 024904 (2004)
- [4] ALICE, (2000), CERN-LHCC-2000-012, ALICE TDR 8.
- [5] ALICE, P. Cortese *et al.*, (2002), CERN-LHCC-2002-016, *Addendum to the ALICE TDR 8*.
- [6] K. Ikematsu *et al.*, (1998), arXiv:physics/9802024 v1.
- [7] F. Geurts *et al.*, Nucl. Instr. Meth. **A508** (2003) 60.
- [8] H. Alvarez-Pol *et al.*, Nucl. Instr. Meth. **A535** (2004) 277.
- [9] CBM Collaboration, *CBM Technical Status Report*, 2006.
- [10] E. Cerron Zeballos, I. Crotty, D. Hatzifotiadou, J. Lamas Valverde, S. Neupane, M.C.S. Williams and A. Zichichi, Nucl. Instr. Meth. **A374** (1996) 132.
- [11] V. Babkin *et al.*, Bulgarian Chemical Communications, **47**, Special Issue-B (2015) 215.
- [12] V. Babkin *et al.*, Nucl. Instr. Meth. **A824** (2016) 490.
- [13] W. Zhu, Yi. Wang *et al.*, Nucl. Instr. Meth. **A735** (2014) 277.
- [14] V.A. Babkin *et al.*, Instr. Exp. Tech., **60**(3) (2017) 307–313.
- [15] V.I. Yurevich *et al.*, Phys. Part. Nucl. Lett. **12** (2015) 778-785.
- [16] V. Babkin *et al.*, 2016 JINST 11 C06007.
- [17] W. Zhu, Yi. Wang *et al.*, Science China Technological Sciences. **56**(11) (2013) 2821.
- [18] F. Anghinolfi *et al.*, Nucl. Instr. Meth. **A533** (2004) 183.
- [19] J. Christiansen, *HPTDC High Performance Time to Digital Converter*, V 2.2 for HPTDC.
- [20] V. Babkin *et al.*, Phys. Part. Nucl. Lett. **13** (5) (2015) 532.
- [21] P. Moreira *et al.*, *White Rabbit: Sub-Nanosecond Timing Distribution over Ethernet*, ISPCS 2009, Brescia, Italy.
- [22] A. Akindinov, A. Alici *et al.*, Nucl. Instr. Meth. **A490** (2002) 58.
- [23] <http://www.wiener-d.com/sc/power-supplies/mpod--lvhv/mpod-lv-module.html>
- [24] J-M. Chaize *et al.*, *TANGO - an object oriented control system based on CORBA*, ICALEPCS 1999, Trieste, 1999.